PHYSICS for ECONOMY

Vol. 3, No. 1, 2019

Issued with the consent of the Rector

Editor in Chief
Publishing House of Rzeszow University of Technology
Grzegorz OSTASZ

Composition of the Scientific Papers Council
of the Faculty of Mathematics and Applied Physics
of Rzeszow University of Technology
„Physics for Economy”
Tomasz WIĘCEK – chairman (Poland)
Dorota JAKUBCZYK – editorial assistant (Poland)

Editor in Chief
Tomasz WIĘCEK (Poland)

Editorial Committee (Thematic editors)
Henryka CZYŻ (Poland)
Vitalii DUGAEV (Poland)
Czesław JASIUKIEWICZ (Poland)

Statistical editor
Andrzej WASILEWSKI (Poland)

Members of editorial staff
Michał INGLOT (Poland), Ryszard STAGRACZYŃSKI (Poland)
Gaweł ŻYŁA (Poland)

Project of the cover
Bożena ŚWIDER

The printed version of the Journal is an original version.

p-ISSN 2544-7742
e-ISSN 2544-7750

Publisher: Publishing House of Rzeszow University of Technology
Powstańców Warszawy 12, 35-959 Rzeszow (e-mail: oficyna@prz.edu.pl)
http://oficyna.prz.edu.pl

Editorial Office: Rzeszow University of Technology, The Faculty of Mathematics and Applied Physics,
Powstańców Warszawy 8, 35-959 Rzeszów (e-mail: phyeco@prz.edu.pl)
Additional information and an imprint – p. 67

TABLE OF CONTENTS

Magdalena KULIG: High-energy transformer's safety 5

A. KUŁAK, K. SUPRYNOWICZ, J. PISAREK: Luminescent powder technique in electronic speckle pattern photography 15

A.A. MIKHAL, D.V. MELESHCHUK, Z.L. WARSZA: Application of the hybrid balanced ratiometric measurement method in the high-precision ac thermometry bridges 29

Tomasz SZCZEPAŃSKI, Sylwia KUDŁA: Resonant tunnelling diode with magnetised electrodes 41

Igor TRALLE, Paweł ZIĘBA: On the new types of composite metamaterials 53

Magdalena KULIG[1]

HIGH-ENERGY TRANSFORMER'S SAFETY

Based on many advantages of fiber optic sensor technology, the article presents the possibility of measuring temperature in difficult environmental conditions, for example in a high electromagnetic field. Fabry-Perot interferometers with a short resonant cavity of low resolution are used in these fiber-optic sensors. The advantages of such a solution include simple and compact construction, low price, low temperature effect and no interference loss due to polarization.
Due to the potential of transformer loads, electrical power plants and operating companies test power transformers to assess their condition, set a schedule for maintenance work and plan replacement. Oil temperature measurement is most commonly used using typical sensors. However, this measurement does not reflect the temperature of the winding during the sudden increase in the transformer load.
The proposed method of verifying the parameter, which is the winding temperature, can be very attractive for electricity distributors.

Keywords: power transformer, winding failure, blackout

INTRODUCTION

High energy transformers are among the most valuable equipment of electrical power plants. The production of new transformers and their delivery to the place of operation generates significant costs, however, damage caused by the transformer failure and consequent loss of electricity production may in consequence be much more serious. Therefore, the plants try to maintain the efficiency of the transformers as long as possible. The life of the transformers depends largely on the winding's operating temperature, so it is important to monitor it.

The unique properties of fiber optics, such as the very large information capacity, the ability to transmit signals over long distances, high information rates, insensitivity to electromagnetic interference and reliability make them widely used in telecommunications, signal processing and measuring technology. Fiber optic temperature sensors are measuring transducers that receive information about the measurement size which is the temperature and process it at the transducer output causing an optical signal.

The work presents a method of temperature monitoring in the presence of high electromagnetic radiation using optical fiber sensors. The special technology

[1] Corresponding author: Magdalena Kulig, Rzeszow University of Technology, Powstancow Warszawy 8, 35-959 Rzeszow, Poland, e-mail: m.kulig@prz.edu.pl

of semiconductor crystals plays an important role in metrology. A method of measuring a sensor based on the use of the Fabry-Pérot interferometer has been proposed.

1. PHYSICAL DESCRIPTION OF THE OPERATION OF A FIBER OPTIC SENSOR

The main component of the measurement system is a fiber optic sensor made in gallium arsenide technology. A great advantage of using gallium arsenide in the device is that it generates less noise than most other types of semiconductors. The gallium arsenide is also completely resistant to electromagnetic induction.

The operating principle of the fiber optic temperature sensor used in the tests is based on the Fabry-Pérot interferometer technology. It is based on the interference of light waves carrying information about temperature. This phenomenon is shown in Figure 1.

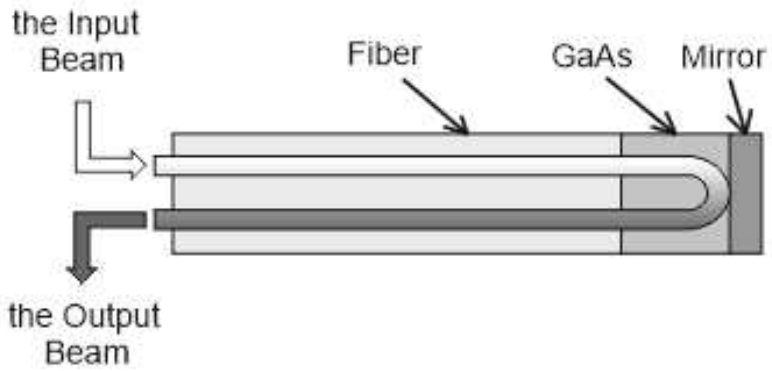

Figure 1. Schematic of the sensor operation based on gallium arsenide technology [1]

A multimode optical fiber uses a continuous broadband light source to illuminate a semiconductor crystal [2-5]. The electrons of the valence band can collide elastically with photons with sufficient energy, which allows to jump to the conduction band. Both bands are separated by an energy gap (E_g expressed in eV). E_g depends not only on the semiconductor structure, but also the hydrostatic pressure and temperature as presented in equation (1) and (2) respectively:

$$E_g(P) = E_g(0) + b \cdot P - c \cdot P^2 \tag{1}$$

where P is the pressure expressed in GPa and for gallium arsenide at 300K:

- $E_g(0) = 1{,}43 \pm 0{,}01\ eV$,
- $b = (10{,}8 \pm 0{,}3)\ eV/GPa$,
- $c = (14 \pm 2) \cdot 10^{-3}\ eV/GPa^2$.

$$E_g(T) = E_g(0) - \frac{\alpha T^2}{\beta + T} \tag{2}$$

where T is the temperature expressed in K ($0K < T < 10^3 K$) and for GaAs at normal pressure:

- $E_g(0) = 1{,}519\ eV$,
- $\alpha = 0{,}541 \cdot 10^{-3}\ eV/K$,
- $\beta = 204\ K$.

Photons, deriving from a continuous broadband light source, illuminating a semiconductor, can interact with valence electrons depending on their energy:

$$E_\gamma(\lambda) = \frac{h \cdot c}{e \cdot \lambda} \approx \frac{1239{,}84}{\lambda} \tag{3}$$

where:

- E_γ is the energy of the photon expressed in *eV*,
- λ is the wavelength of the photon expressed in *nm*,
- h is the Planck constant,
- c is the speed of light in a vacuum,
- e is the absolute value of the elementary charge of the electron.

Photons with longer wavelength has lower energy. These photons passed through the semiconductor, return to the optical sensor after reflection from the mirror limiting the system. Only photons with higher energy ($E_\gamma > E_g$) are absorbed. A resultant form of the high pass filter in the wavelengths shown in Figure 2.

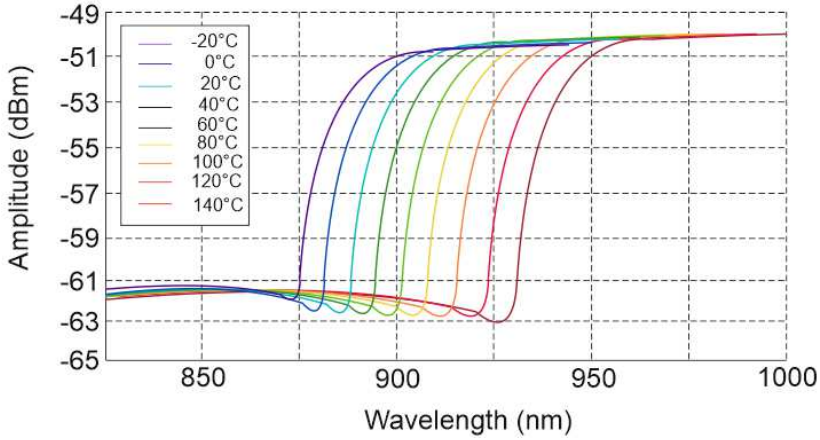

Figure 2. The GaAs sensor spectrum measured by an optical spectrum analyzer at temperatures from -20 to +140 with a difference of 20 [3]

The measurement by means of a fiber optic sensor is based on the use of the Fabry-Pérot interferometer (IFP). Interference image is obtained due to the resonance cavity. In a flat IFP, a parallel beam of light can bounce repeatedly from flat mirrors arranged in parallel or not bounced at all. All rays (reflecting and not reflecting) interfere with each other giving a contribution to the resultant intensity of light passing through IFP. The light intensity at the exit is determined by the formula:

$$I = \frac{I_0}{1+Fsin^2\Phi} \tag{4}$$

where Φ is the phase delay produced by the beam passing through the resonance cavity once, while the

$$F = \frac{4R}{(1-R)^2} \tag{5}$$

is called the slenderness coefficient of interference fringes, R denotes the intensity of reflection coefficient of mirrors [6].

The unique design of the sensor is based on the measurement of the cut-off of the wavelengths of light. Temperature variations create differences in the wavelengths cut off in the Fabry-Pérot cavity and the signal conditioner can continuously measure the wavelength with high accuracy despite any unfavorable environmental conditions (electromagnetic interference, humidity and vibration). Through the use of cross-correlation of white light, signal meters have a surprising speed, providing very accurate and reliable measurements. The principle of IFP's operation is shown in Figure 3.

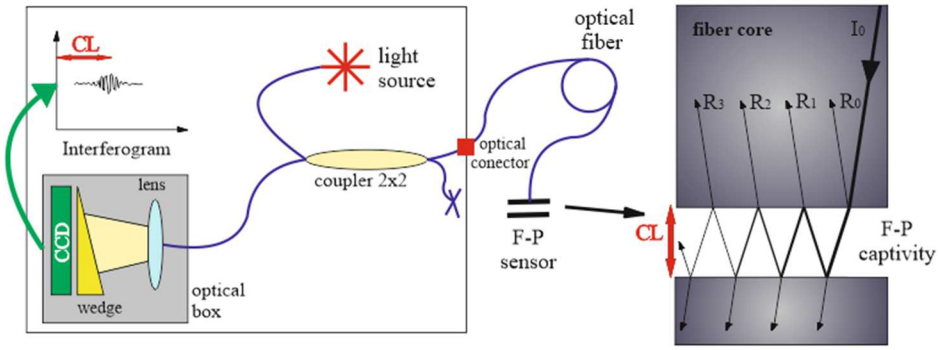

Figure 3. Schematic description of the F-P absolute measurement signal based on white light interference (left) and the structure of the F-P measurement interferometer showing the course of rays obtained by the propagation of the light beam in the optical fiber core (right) [3]

The TPT-62 probe is a robust, fiber-optic temperature probe for use in oil-filled power transformers. It is specially designed to withstand transformer operation conditions, including desorption of kerosene and heat and vibration release during the entire life of the transformer. The geometrical parameters of the sensor are shown in Figure 4:

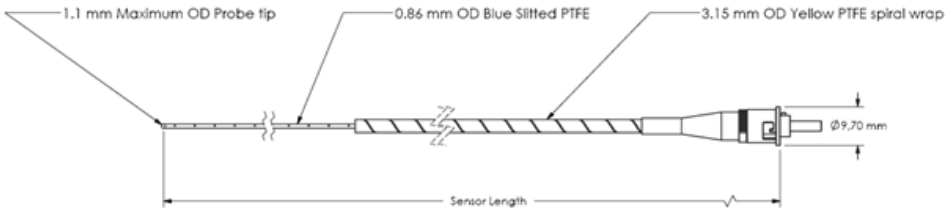

Figure 4. The construction of the TPT-62 measuring probe [1]

The temperature range of the TPT-62 sensor ranges from –40°C to 225°C, 0.1°C resolution, and temperature accuracy of ± 1°C.

Fiber optic sensor is made of insulating materials and is insensitive to electromagnetic interference.

2. HIGH-ENERGY TRANSFORMER TESTING

Power transformers transform electrical energy from one voltage level to another - they increase the transmission voltage to limit losses or power interruptions in the distribution network. The lifetime of the transformers depends largely on the winding operating temperature (Figure 5).

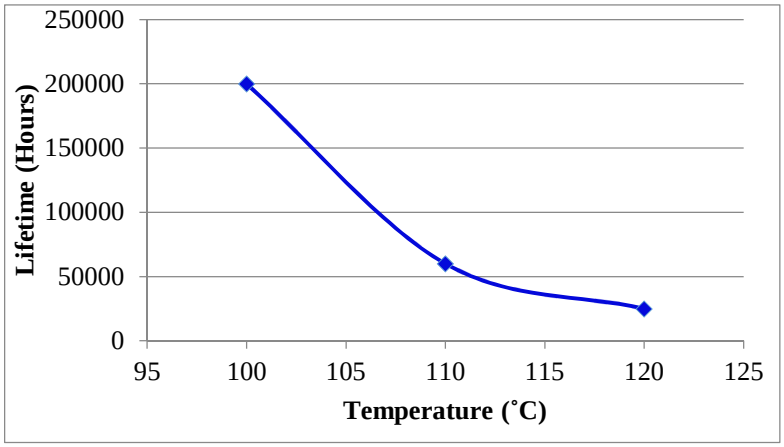

Figure 5. Influence of transformer winding temperature on its lifetime

Internal losses, caused mainly by the load current, have to be discharged. High temperature causes deterioration of transformer insulation materials. Transformer damage caused by these interactions can cause explosion, fire and costly consequences, such as prolonged downtime due to the need to clean and repair the site, as well as the need to wait for new transformers to be delivered.

Figure 6 shows the image of a damaged transformer.

Figure 6. A damaged high-energy transformer

3. THE EXPERIMENTAL METHOD

Testing high power transformers in laboratory conditions is difficult due to the costs. In order to familiarize with the phenomenon from the experimental side, a low power transformer (50W) was tested, immersed in silicone oil [7]. The diagram of the measurement station is shown in Figure 7. One of the sensors measures the temperature directly on the winding, the other measures the oil temperature. The measuring system works via the Nortech Sentinel II interface with a computer program that has the ability to record temperature changes over time. The dynamics of oil temperature changes and the winding of the transformer immersed in it at an exemplary overload 250W is shown in Figure 8.

As can be seen, there are significant differences in the temperature of the winding compared to the oil temperature at a rapid increase in the load. It follows from this conclusion that the oil temperature measurement alone does not show the actual operating condition of the transformer and the temperature measurement should be used directly on the winding. In addition, measuring the temperature in several places of the winding allows to detect the initial phase of damage,

for example compact coils and gives the possibility of switching off the transformer before its complete destruction.

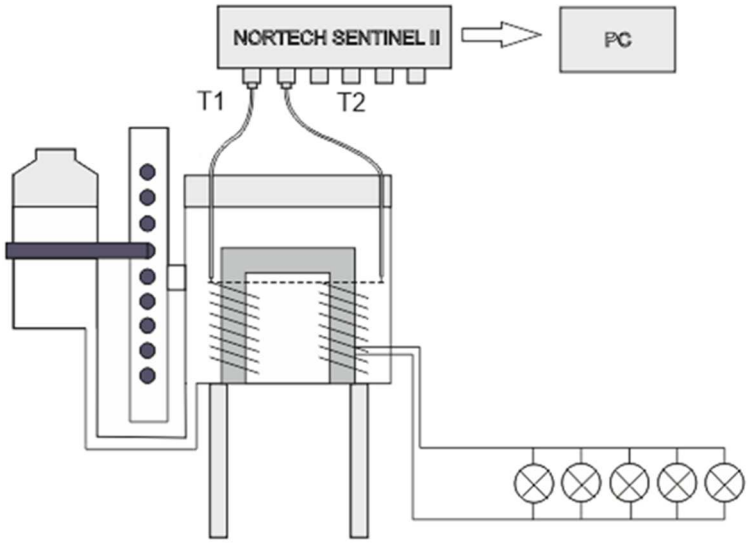

Figure 7. The scheme of measurement

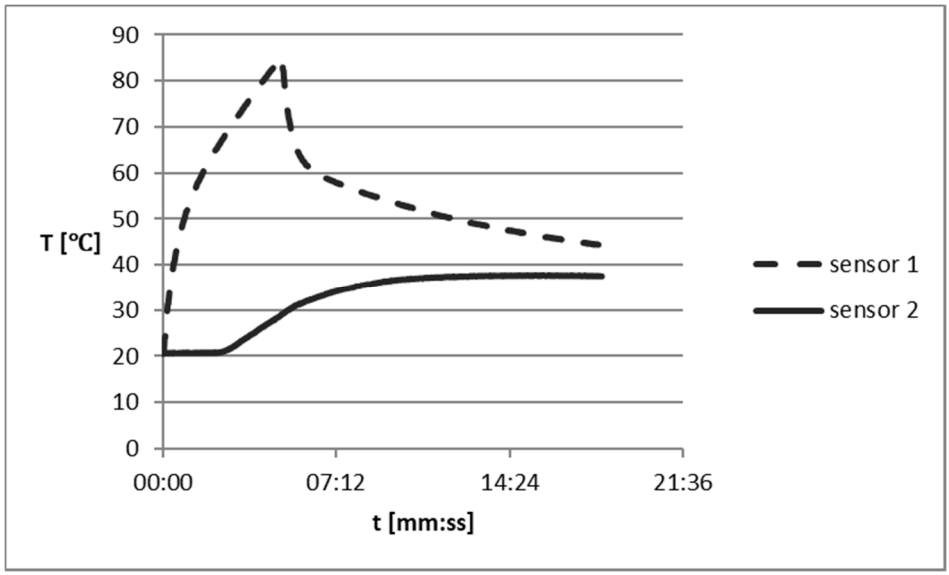

Figure 8. Dynamics of oil and winding of the transformer immersed in oil temperature changes; sensor 1 - winding temperature measurement, sensor 2 - oil temperature measurement

4. CONCLUSIONS

The paper proposes an experiment that allows for temperature measurement in unfavorable environmental conditions. The sensor proved itself and correct measurements were taken in real time.

In the experiment carried out to measure the temperature of the transformer winding and electro-insulating liquid, which was silicone oil as an insulator and coolant of the power transformer. The measurements showed ineffectiveness of the traditional temperature measurement of the oil itself. Spontaneous convection of fluid was noticed, which could additionally confuse potential users and mask the actual temperature of the winding. The presented method of transformer monitoring is extremely useful for electric energy distributors.

REFERENCES

[1] www.fiso.com.

[2] Pinet E., Fabry-Perot Fiber-Optic Sensors for Physical Parameters Measurement in Challenging Conditions, Journal of Sensors 2009.

[3] Pinet E., Ellyson S., Borne F., Temperature fiber-optic point sensors: Commercial technologies and industrial applications, FISO Technologies

[4] Bass M., Mahajan V. N., Handbook of Optics, Third Edition Volume I, The McGraw-Hill Companies, Inc., New York 2010

[5] Tang J., Fiber-Optic Measurement Systems: Microwave and Radio Frequency Heating Applications, Encyclopedia of Agricultural, Food and Biological Engineering, Marcel Dekker 2006

[6] Kaczmarek Z., Światłowodowe czujniki i przetworniki pomiarowe, Agenda Wydawnicza PAK, Warszawa 2006

[7] Zagrobelna M., Wasilewski A.; Power transformer testing, Proc. of SPIE Vol. 9290, Photonics Applications in Astronomy, Communications, Industry, and High-Energy Physics Experiments 2014

MONITOROWANIE TEMPERATURY TRANSFORMATORA WYSOKOENERGETYCZNEGO Z WYKORZYSTANIEM CZUJNIKA ŚWIATŁOWODOWEGO

Bazując na wielu zaletach technologii czujników światłowodowych, artykuł przedstawia możliwość pomiaru temperatury w trudnych warunkach środowiskowych, na przykład w wysokim polu elektromagnetycznym. W omawianych czujnikach światłowodowych stosuje się interferometry Fabry-Perota, z krótką wnęką rezonansową o małej rozdzielczości. Walorami takiego rozwiązania są m.in. prosta i zwarta budowa, niska cena, mały wpływ temperatury oraz brak zaniku obrazu interferencyjnego wywołanego polaryzacją.

W związku z możliwością obciążeń transformatorów, zakłady elektroenergetyczne oraz firmy prowadzące eksploatację testują transformatory mocy w celu oceny ich stanu, ustalenia harmonogramu prac konserwacyjnych i zaplanowania wymiany. Najczęściej stosowany jest pomiar temperatury

oleju stosując typowe czujniki. Jednak taki pomiar nie odzwierciedla temperatury uzwojenia podczas nagłego zwiększenia obciążenia transformatora.
Zaproponowany sposób weryfikowania parametru jakim jest temperatura uzwojenia może być bardzo atrakcyjny dla dystrybutorów energii elektrycznej.

Keywords: transformator mocy, uszkodzenie uzwojenia, blackout

DOI: 10.7862/rf.2019.pfe.1

Received:17.04.2019
Accepted:30.05.2019

A. KUŁAK[1]
K. SUPRYNOWICZ[2]
J. PISAREK[3]

LUMINESCENT POWDER TECHNIQUE IN ELECTRONIC SPECKLE PATTERN PHOTOGRAPHY

For the generation of speckle images, a luminescent powder applied in a small amount to the sample surface and stimulated by UV radiation was used. We obtained fine-grained speckle patterns with very high contrast and small size of spots, The shape of the single speckle, unlike laser method, is circular, which is important for the effectiveness of the used digital image analysis methods. The measurements of displacements and deformations were made by use of digital image registration and its analysis using correlation procedures. The results are presented in the form of bitmaps, tables and graphs. The developed method was tested on flat wood specimens subjected to three-point bending.

Keywords: speckle metrology, elektronic speckle, ESPI, white light speckle photography, experimental strain analysis, analize of speckle pattern, speckle pattern, luminescent powder

INTRODUCTION

The laser speckle analysis of deformations of structural elements is known from the 80s of the last century [2-6, 10, 11] and it is always connected with a measurement error resulting from the rotation or deformation of the analysed surface. The speckle pattern recorded in laser light is spatial and during loading of the object it performs two movements simultaneously:

- translatory motion related to the linear displacement of the analysed part of the object's surface,
- rotary motion associated with the rigid rotation of the body and the local deformation of its surface.

[1] Jan Długosz University in Częstochowa, Institute of Technology and Safety Systems, Al. Armii Krajowej 13/15 42-200 Częstochowa – student
[2] Warsaw University of Technology, Institute of Aeronautics and Applied Mechanics, Nowowiejska 24, 00-665 Warsaw, Poland, E-mail: ksuprynowicz@meil.pw.edu.pl
[3] Private laboratory of experimental mechanics, ul. Kiedrzyńska 95 m 20, 42-200 Częstochowa, e-mail jerzy.pisarek@gmail.com , tel.+48 601842074

The linear displacement of the speckle registered by the camera is a superposition of displacements resulting from both movements. The difference between the real vector displacement of the selected point and its image recorded by the camera is proportional to the vector product $\Delta s = \boldsymbol{\delta} \times \mathbf{d}$ of the local rotation angle $\boldsymbol{\delta}$ and the local defocusing vector **d**. This is illustrated in Fig. 1.

The displacement's vector "s" recorded by the CCD camera is a view on the object plane as the sum of vectors **s** and $\Delta\mathbf{s}$. Regardless of the errors discussed above the spatial character of speckle structures generated in laser light leads to blurring of recorded images and lowering their contrast, which may result in a high level of random errors associated with the numerical processing of speckle images.

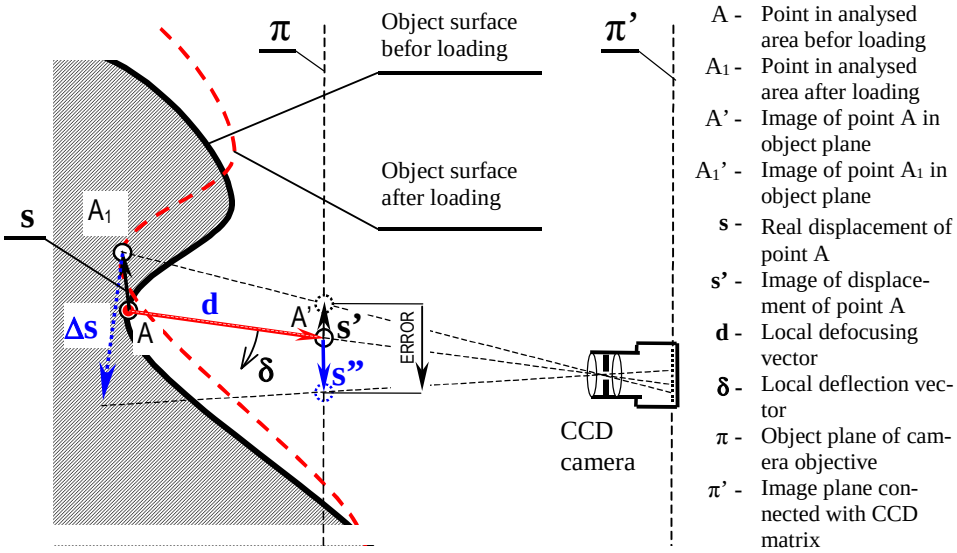

Fig. 1. Error recorded by the camera of the mapping of the actual displacement of the selected point A. It was caused by the camera's focusing and the rotation of the coherent speckle structure by the angle **δ**.

Numerical analysis of speckle positions in coherent method is also hampered by irregular shapes of speckles. This is visible in Figure 2.

The uniqueness and complexity of the speckle shapes materially impedes both initial and final selection of features used for tracking position of selected area of film frame or bitmap.

Problems related to the separation of linear deformations or strain and problems related to the industrial application of laser metrology have resulted in the development of methods of speckle metrology in white light [12-14, 20, 24]. One of the variants of this group of measurement methods is the technique of reflective powders developed by J. Pisarek [7, 8], based on spraying of reflective powder

(most preferably dactyloscopy powder) on the surface of tested object. The disadvantages of this technique are:

- necessity of blackening the surface of the object before applying dust to it,
- relatively low durability of the dust layer,
- necessity of using strong light sources with a fairly high spatial coherence.

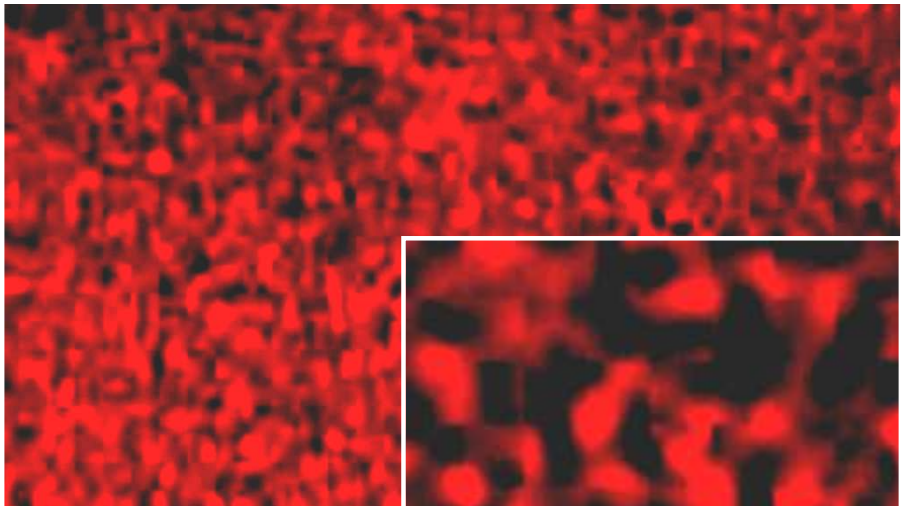

Fig. 2. Speckle pattern generated by the wood surface in the light of the GaAS laser

In order to obtain a high contrast of speckle structures and to eliminate uneven illumination of recorded images, it is necessary to work in the dark, which may be troublesome in industrial or range environments. An alternative to powder technology [7, 8] is the use of special reflective paints containing salt crystals (C.Forno [12]) or glass microspheres. The preparation and proper use of these paints is quite cumbersome and requires practical experience. The luminescent powder technology proposed in this article is much easier to use in practice. The analysis of speckle pattern (and specklegrams) can be making using analogue methods, like optical Fourier processors [3, 6-8, 14, 20, 24] or digitally with the use of different techniques of the image analysis. In the literature one can find a great deal of examples of uses of the digital analysis application e.g. works [9, 18, 19, 22, 23, 30-37]. The number of original works concerning of the methodology of research [25-29, 38] is evidently smaller. Measuring techniques presented in this article were checked experimentally within the framework of the work [1] realised in the Institute of Techniques and Systems of Safety in the Laboratory of Speckle Metrology, Holography and the Optical Information Processing and partially in the private laboratory of the experimental mechanics founded by

J. Pisarek. Calculations were performer by use of the author's programming [15, 17] developed by K. Suprynowicz.

1. PRINCIPLES OF EXPERIMENTAL TECHNIQUE

The essence of the proposed techniques is the sprinkling of luminescent or phosphorescent powders into object's surfaces. Authors propose the following dust application techniques:

- powder spraying and gravitational descending on a dry surface of the element,
- powder spraying and gravitational descending on the surface of the element covered with wet paint, oil or other sticky substance,
- spraying the surface with a clear varnish containing a luminescent active pigment.

Depending on the type of luminescent or fluorescent powder used, the surface of the element is irradiated with UV light or visible light with a wavelength shorter than the light emitted by the dust. In the case of fluorescent powders the image exposure was done immediately after lighting. In second case with using of luminescent powders - exposure was done in during of a photoexcitation so an addition of UV filter to the camera's optical pathway was necessary.

1.1. Preparation of specimens surfaces

The tests were carried out on flat wooden specimens. Obviously, the same methodology can be used for any structural material and elements of any shape. A hair sprayer was used to spray the powder. Construction of a simple sedimentation chamber was required to obtain an even distribution of marker particulate. The device is shown in Fig. 3. The chamber should have dimensions much larger than the size of the sputtered element. Authors used cardboard boxes to create a simple and effective chamber.

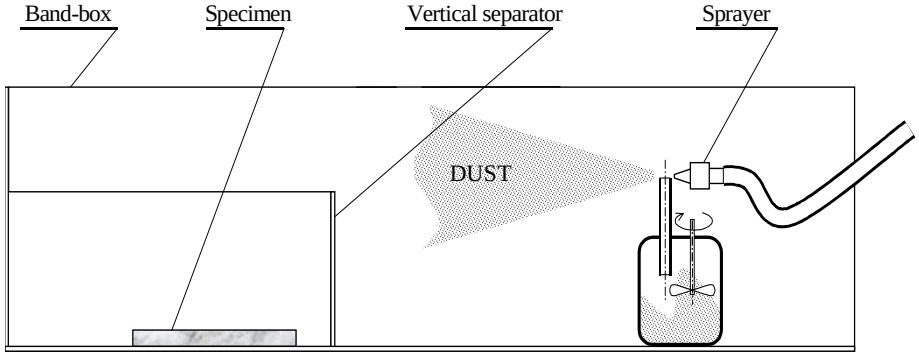

Fig. 3. Sprayer used to cover a wooden specimen

In use of non-transparent coating technology, black acrylic spray varnishes were applied following the manufacturer's instructions. The CAPON clear lacquer (nitro-cellulose lacquer) was applied simply with a brush.

The preparation of the luminescent varnish required the following sequence of operations

1. Pigment distribution in a large amount of solvent (about 0.5 g / l)
2. Dilution of the CAPON varnish in the ratio 4: 1
3. Introduction of varnish to the sprayer or atomiser
4. Spray painting

For the preparation of luminescent varnishes, transparent resins for UV and solvent suitable for their dilution should be used. The best results are obtained by using a methyl methacrylate (plexi) diluted with chloroform with the addition of a small amount of plasticizer (N-N butylphthale) as a resin.

A typical speckle pattern obtained by spraying luminescent powder on wet lacquer layers is shown in Figure 4. Regular shapes of spots deserve the attention, because they enable the application of such tools of the image analysis which in case of laser speckle pattern would be very troublesome.

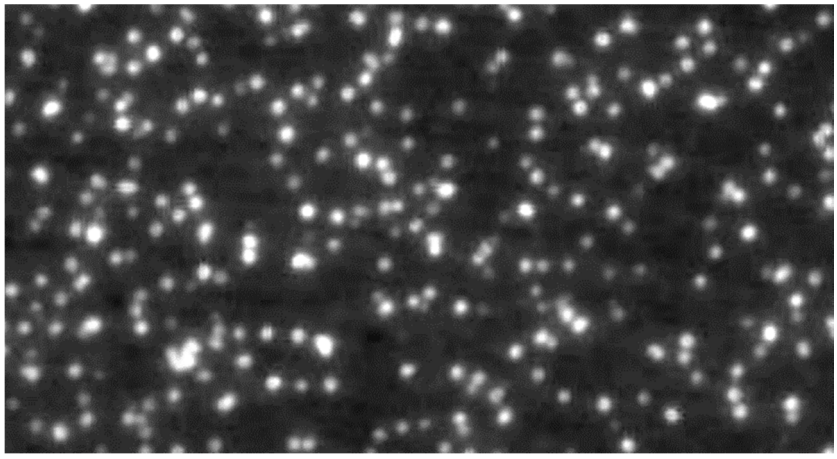

Fig. 4. Structure obtained by spraying by luminescent powder (source [1])

The homogeneity of the background is a second advantage of speckle pattern obtained by luminescent or phosphorescence techniques.

1.2. Registration of the image

The scheme of speckle image capture system is shown in figure 5.

The specimen was illuminated at an angle of about 30^0 with a UV reflector. The camera and the loading system were placed on long strip footing. The diagram of the loading system is shown in figure 6.

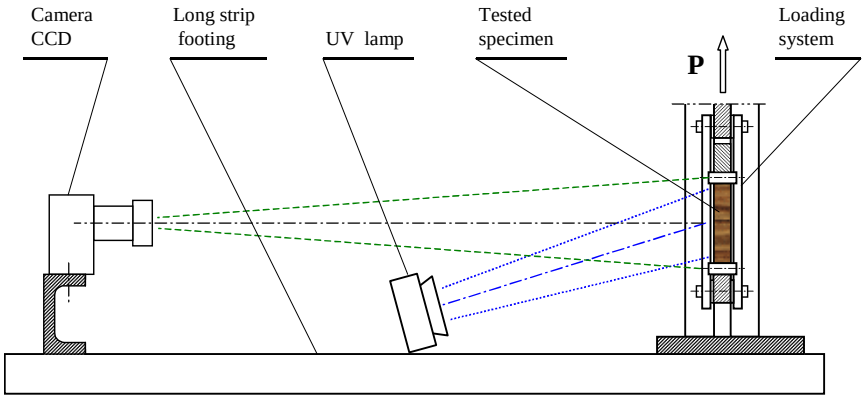

Fig. 5. Scheme of registration system

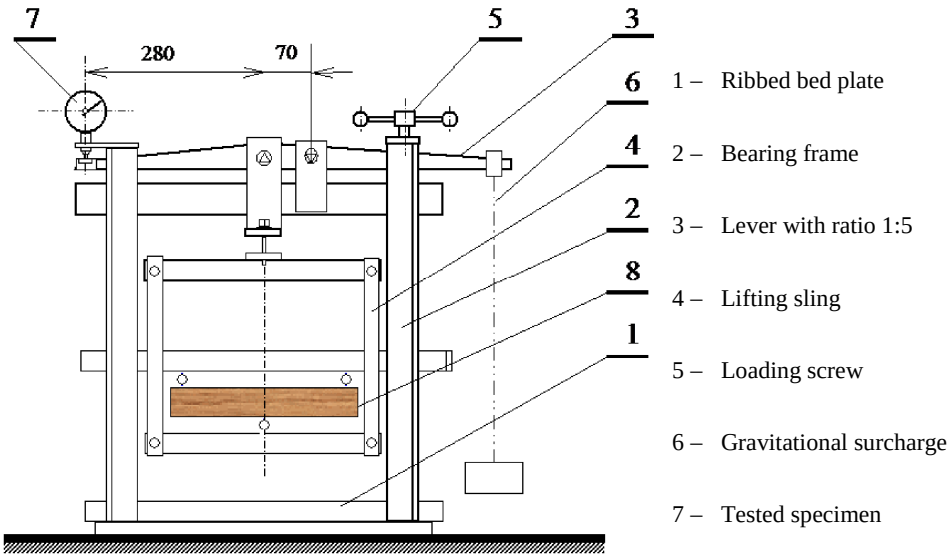

Fig. 6. Configuration of loading system (source [1])

1.3. Loading system

In the experiment the loading system from elastooptic polariscope was used. He enabled the realisation facultative flat states of the strain. The load was realised in a kinematics manner by means of the screw (5). The value of displacement of selected point of the lever (3) was measured with the accuracy about 0.01 mm by means of the dial gauge (7). This made possible to determine the value of displacement of the force application point on accuracy of 0.002 mm. Unfortunately, the low stiffness of the lifting sling and the low stiffness of the benches on which

the entire loading system has been mounted cause additional and uncontrolled movements of the sample relative to the reference system connected with the camera. Compensation of this effect (possible on the way of numerical processing of registered bitmaps) is effective for determination of strain only. Unfortunately, the compensation of systematic errors appearing in measurement of movements is here not possible.

For achievement of this purpose the measurement of movements of apparent elements of the lifting sling would be necessary. Unfortunately authors of this work did not perform this additive measuring.

1.4. Image analysis

Displacement and strain distributions were calculated using two-dimensional Digital Image Correlation software. Software utilises a two-step approach, with first step using rectangular image subset, that is tracked on concurrent images with subpixel precision using bicubic interpolation. Tracking is conducted by a brute force search algorithm maximising Pearson correlation coefficient between two images. Speckles are used as subset centres. First step results in approximate displacement map. Second step of the algorithm begins with creation of triangle mesh with vertices placed on individual speckles. Pearson correlation coefficient is again maximised, this time using algorithm similar to simulated annealing. Strain distribution is derived from the resulting displacement map by calculating finite differences. Strain distribution is then filtered by Gaussian kernel filter.

Regular shapes of speckles obtained with the use of luminescent powders give the possibility of image processing also using the algorithms based on the click theory and the theory of Markov random fields [16]. These methods allow a very significant reduction of accidental error and improve the measurement accuracy by at least an order of magnitude. Unfortunately, they are sensitive to the occurrence of the common errors. Therefore, they should be used in conjunction with correlation methods.

2. APPLICATION IN THE TEST OF COMPOSITE SPECIMENS

The test method were carried out on wooden specimens with the dimensions 250x50x18 mm under three point loading according to the scheme shown in Fig. 7.

Fixed points should exhibit not the true displacements of selected specimen area but present an additional rigid displacements of the recorded image, relative to the camera coordinate system. These movements are a sum of movements related to the deformation of the sample and movements connected with of her rigid turn, resulting from the foldability of the loading arrangement. The second from mentioned components of displacement can be compensated by software in the data analysis process. An additional source of discrepancies in the experimental

results in relation to the theoretical expectations was the non-linearity of the elastic characteristics of wood, and in the case of large loads also its plastic deformations.

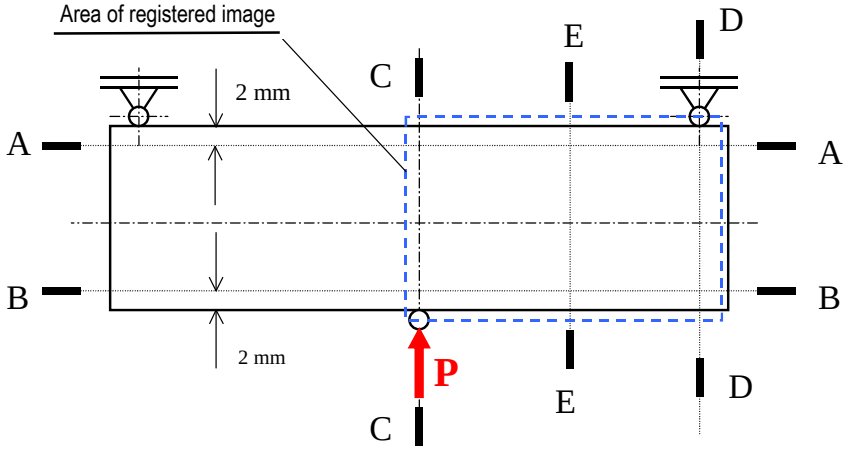

Fig. 7. Diagram of sample loading and position of cross sections for which the deformation distribution are presented in the following part of the article (Figures 11 and 12)

2.1. Whole field results of displacement measuring

The results of the displacements and strains analysis can be presented in whole field in the form of contour diagrams or bitmaps, on which a given value of displacement or strain corresponds to a particular colour of the image. This article adopts a scale in which the smallest value corresponds to the blue colour (the shortest wavelength of light) and the highest value is the red colour (the longest wavelength). Figures 8-10 show a linear mapping of the measured value of the wavelength assigned to a given measuring point. Obviously, due to the requirements of the printing process particular colours are simulated using the superposition of the so called primary colours.

Figure 8 shows colour maps of horizontal and vertical linear displacement, which was measured in a direction perpendicular to the direction of observation.

They conform to the load by the central force P which causes the vertical displacement to be set at the point of its application and accord to the movement of the point of force application equal approx. 4 mm. The dark area near the point of application of force is the shadow of the roller, through which the force is applied to the sample. It is visible due to the angular lighting (below at an angle of about 30^0).

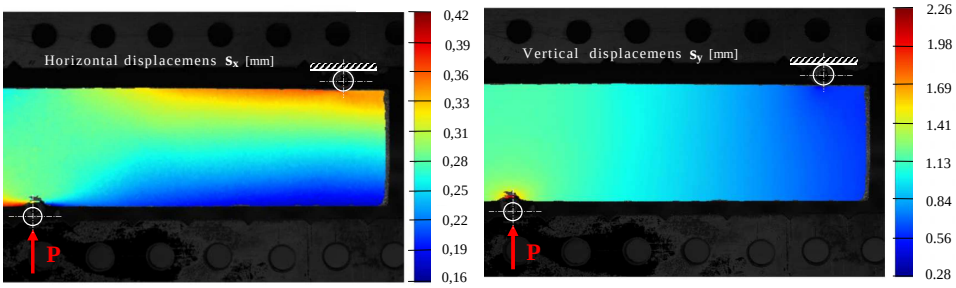

Fig. 8. Experimentally obtained colour maps representing distribution of displa-cements of the wood specimen surface during three-point bending

The following diagrams show the strain distributions ε_x (Fig. 9) and ε_y (Fig. 10) corresponding to the same load. All plots were prepared based on the analysis of the same pair of speckle images, i.e. the image recorded before and after loading the specimen. Fig. 9 shows the characteristic shape of the deformed zone, called "dog bone" in the jargon of people dealing with the strength of materials and with the fracture mechanics. It is characteristic for areas that are plastically deformed. The figure also shows some irregularities in the strain distribution that may be related to the structure of the material being tested These effects will be more clearly visible in point-by-point analysis, the result of which in selected sections is shown later in the work (Figs 11-12).

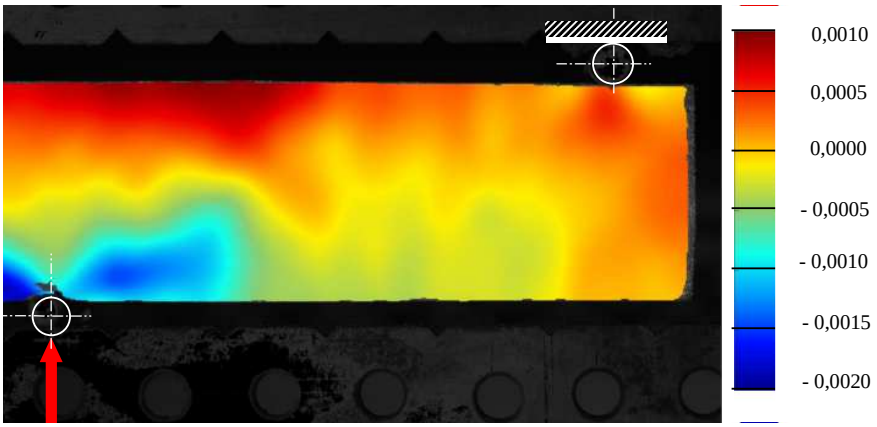

Fig. 9. Bitmap representing distribution of strain ε_x in whole field displacements (source [1])

The distribution of deformations ε_y visible around the point of application of force (Fig. 10) resembles the distribution of equivalent stresses known from the classic elastic theory, calculated according to the Mohr hypothesis.

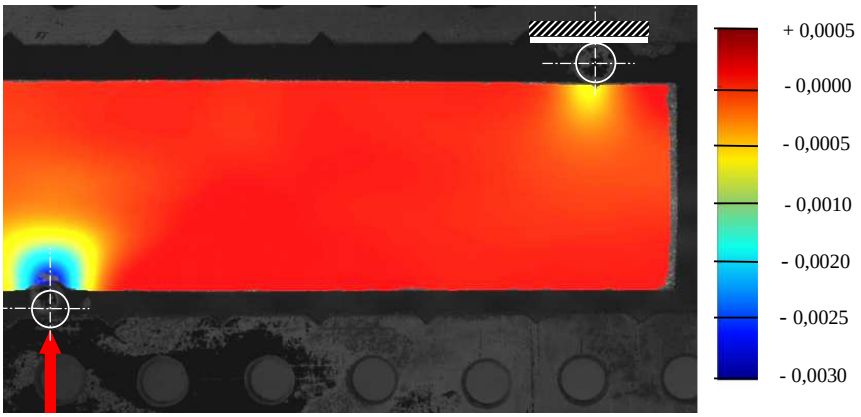

Fig. 10. Bitmap representing distribution of strain ε_y in whole field (source [1])

2.2. Strain distribution in selected cross-sections

On figure 11 the deformation distributions corresponding to different values of the shift of point of force application, and resultative different loads were compared. It quite unexpectedly turned out that the deformations measured locally are not proportional to the load and change irregularly along the cross-section. This is undoubtedly due to the nature of the material used for the tests, which is not linear-elastic, and, moreover, has a significant dispersion of local properties. So what is the sense to performing the engineering calculations with FEM, where the so-called simplifying assumptions are evidently leading to false results?

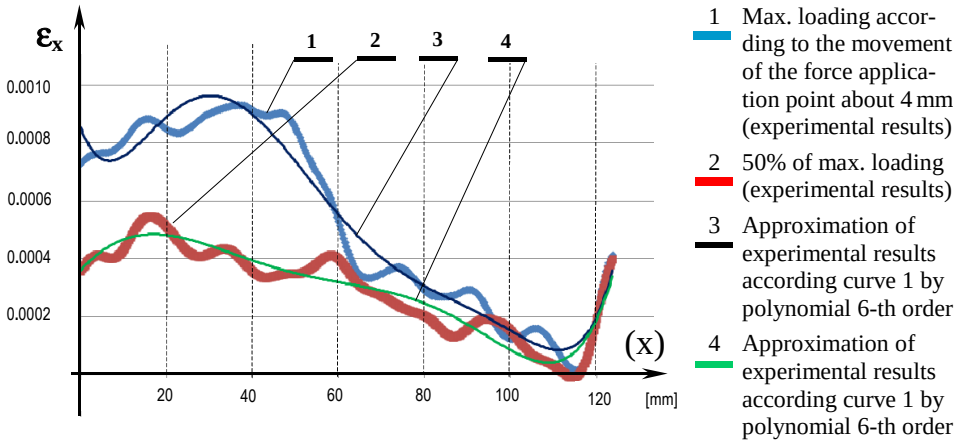

Fig. 11. Distribution of linear strains ε_x along the A-A section from fig. 7 (date from [1])

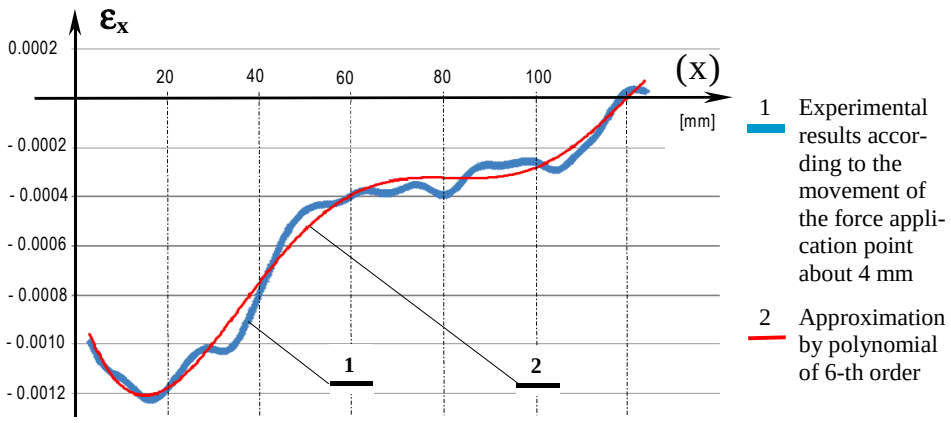

Fig. 12. Distribution of linear strains ε_x along the B-B section from fig. 7 (date from [1])

The graph shown in Fig. 12 shows only a few percent fluctuations of locally measured values (presented by a blue-green curve) around average values (red curve). Drastic differences in the course of diagrams of strains measured relative to perpendicular axes suggest a clear effect of the positioning of the composite fibres on the measurement result. Thanks to the measurement technique described in the article, it is possible to experimentally verify the actual impact of numerical errors (especially FEM calculations) on computational errors and validation of the software used.

CONCLUSIONS

The technique of speckle photography based on the use of luminescent powders is insensitive to angular displacements and angular micro-deformations of the tested object. It can be used on any elements without the need to blacken them. The phosphor may be applied by sputtering or introduced into the outer layer of the varnish coat. The second of presented techniques makes the method proof to atmospheric factors and its effective also in open area or range conditions. Due to the separation of pigment grains and their small size the luminescence technique combined with numerical image processing based on correlation techniques allows to achieve a resolution of several dozen μm are used. At the same time, the regular circular shape of the speckles creates favorable conditions for the use of image analysis techniques based on the theory of Markov random fields and clique theory, which should increase the measurement accuracy by an order of magnitude.

The simplicity of technology, a very wide measuring range and the ability to analyze deformations at very small measuring bases predestine the technique described for use as a basic experimental way of validating numerical engineering

programs, including FEM programs. In the case of using varnish coatings, an additional argument in favor of the use of the measurement technique described in the article for validation and technical inspection is random and practically unique spatial distribution of spots recorded on a bitmap, which makes it practically impossible to make undetectable falsifications. An additional argument for the widespread use of the described technique supplemented with a possibly more extensive data analysis system is availability and a very low cost of measuring equipment and consumables.

LITERATURE

1. A. Kułak – „*Analiza stanów odkształcenia próbek drewnianych poddanych zginaniu trójpunktowemu*" praca dyplomowa UJD 2019 (dostęp przez APD UJD)
2. Goodman J.W. – *„Statistical properties of laser speckle patterns"* In: Dainty JC, editor. Laser speckle and related phenomena. Berlin: Springer Verlag; 1975. p. 9–19775.
3. Erf R.K. – „*Speckle metrology"* - London: Academic Press; 1978.
4. Stetson J.A. – „*A review of speckle photography and interferometry"* Opt Eng 1975;14:482–9.
5. Rene Skov Hansen –„A compact ASPI system for displacement measurements of specurar reflecting or optical rough surfaces" – Optics and Lasers in Engineering41 (2004), p.73-80
6. M.Francon - *„Оптика спеклов"* - изд. МИР,Москва 1980 (тлум. Ю.Островски)
7. J.Pisarek – „Doświadczalna analiza przemieszczeń i odkształceń metodami fotografii plamkowej w świetle białym" – rozprawa doktorska – Częstochowa 1987
8. J.Pisarek – „Оптико-цифрові методі і системі аналізу спеклограм для визначения полів перемещеь і дефщрмацій" = **„**Optyczno-cyfrowe metody analizy specklogramów prowadzące do wyznaczenia pól przemieszczeń i odkształceń." Lwów 1996
9. Chen D.J., Chiang F.P., Tan Y.S., Don H.S., „*Digital speckle displacement measurement using a complex spectrum method*" Appl Opt 1993;32:1839–49.
10. Burch J.M., Tokarski J.M.J., „*Production of multiple beam fringes from photo graphic scatters*" Opt Acta 1968;15:101.
11. Archbold E., Ennos A.E., „*Displacement measurement from double exposure photography*".-Opt Acta 1972;19:253–71.
12. C. Forno, „*White light speckle photography for measuring deformation, strain and shape*" - Opt. and Laser Techn. oct.1975. s. 217-221
13. W.Bachmacz, J.Pisarek-"*Determination of Displacements of Plates and Shells by means of White Light Speckle Method*"- 8-th Congress on Material Testing, Budapest 1982, p. 881-884
14. Pisarek- "*The Range and Precision of White Light Speckle Photography*"- *Fracture Mechanics - FMC Series* No.26/1987, Seiten 147-155
15. Bielawski Radosław, Kowalik Michał, Suprynowicz Karol [i in.]: *„Experimental study on the riveted joints in glass fibre reinforced plastics (GFRP)"*, w: Archive of Mechanical Engineering, vol. 64, nr 3, 2017, s. 301-313

16. M.A. Kojdecki, *"O metodzie regularyzacji Tichonowa i przybliżonym rozwiązywaniu liniowych zagadnień niepoprawnie postawionych*"- mat. *„II Seminarium Metod Matematycznych Analizy obrazów Prążkowych"* Częstochowa 1993, str.67-75
17. K. Suprynowicz, "*Opracowanie optycznej metody wyznaczania pola odkształceń próbek pierścieniowych i jej wykorzystanie do badań właściwości mechanicznych tętnic*" = ang: "*Development of optical method for determining strain distribution in ring-shaped aorta specimens and its application for determining mechanical properties of aorta'* – MEL Warszawa 2018
18. F. Labbe, *„Strain-rate measurements by electronic speckle-pattern interferometry (ESPI)"* Optics and Lasers in Engineering 45 (2007) 827–833, www.elsevier.com/locate/optlase
19. Fu-Pen Chiang, *„Super resolution digital speckle photography for micro/nano measures"* – Optics and laser Engineering 47 (2009), 274-279
20. Marcel Dekker, "*White Light Speckle Metrology*", in *Speckle Metrology*, ed. R. S. Sirohi, Inc. Chap. 7, 325-371, 1993.
21. Pramod K. Rastogi, *„An Electronic Pattern Speckle Shearing Interferometer for The Measurement of Surface Slope Variations of Tree-Dimmensional Objects"* – Optics and Laser in Engineering 26 (1997) 93-100 ©Elservier
22. Dieter Dirksena, Jan Gettkant, Guido Bischoffb, *„Improved evaluation of electronic speckle pattern interferograms by photogrammetric image analysis*" Optics and Lasers in Engineering 44 (2006) 443–454
23. Wu X.P., *„Laser and white light speckle techniques in experimental mechanics"* In: 2nd national congress exp. mech. Tianjing, China: Chinese Society ofMechanics; August 1980.
24. Asundi A., Chiang F-P. *„Theory and applications of the white light speckle method for strain analysis"* - Opt Eng 1982;21:570–80.
25. Chiang F.P., *„Electron speckle photography. Some recent advances"* Proc. Speckle 06: speckles, from grains to flowers. SPIE 2006;6341:1–5.
26. Chen D.J., Chiang F.P., *„Computer-aided speckle interferometry using spectralamplitude fringes"*- Appl Opt 1993;32:225–36.
27. Chen D.J, Chiang F.P., Tan Y.S., Don H.,S., *„Digital speckle displacement measurement using a complex spectrum method"* - Appl Opt 1993;32:1839–49.
28. D. Lecomptea, A. Smitsb, Sven Bossuytb, H. Solb, J. Vantommea, D. Van Hemelrijckb, A.M. Habrakenc, *„Quality assessment of speckle patterns for digital image correlation"* - Optics and Lasers in Engineering 44 (2006) 1132–1145
29. Jin Guanchanga, Wu Zhena, Bao Nikengb, Yao Xuefen, *„Digital speckle correlation method with compensation technique for strain field measurements"* - Optics and Lasers in Engineering 39 (2003) 457–464
30. K.M. Abedin, M. Wahadoszamen, A.F.M.Y. Haider, *„Measurement of in-plane motions and rotations using a simple electronic speckle pattern interferometer*" - Optics & Laser Technology 34 (2002) 293–298 www.elsevier.com/locate/optlastec
31. X.F. Yaoa, L.B. Menga, J.C. Jina, H.Y. Yeh, *„Full-field deformation measurement of fiber composite pressure vessel using digital speckle correlation method"* - Optics and Lasers in Engineering 41 (2004) 73–80 Optics & Laser Technology 35 (2003) 639–643 www.elsevier.com/locate/optlastec

32. Kyung-Suk Kima, Ki-Soo Kangb, Young-June Kangc, Seong-Kyun Cheongd, *„Analysis of an internal crack of pressure pipeline using ESPI and shearography”* - Optics & Laser Technology 35 (2003) 639–643 www.elsevier.com/locate/optlastec
33. Carlos Perez Lopez, Fernando Mendoza Santoyoa, Ramon Rodrigez Veraa, Marcelo Funes Gallanzib, *„Separation of vibration fringe data from rotating object fringes using pulsed ESPI”* Optics and Lasers in Engineering 38 (2002) 145–152
34. Ferenc Gymesi, Szabolcs Mike, „*One-wavelength in-plane rotation analysis in electronic speckle pattern interferometry*” - Optics and Lasers in Engineering 35 (2001) 33-40
35. Linda Larssona, Mikael Sjodahl, Fredrik Thuvanderb, „*Microscopic 3-D displacement field measurements using digital speckle photography*” - Optics and Lasers in Engineering 41 (2004) 767–777
36. Jean-Pierre de Vaujany, Michele Guingand, "*EPSI validation for cylindrical gears*”- Optics and Lasers in Engineering 42 (2004) 447–459
37. Adrian U.J. Yapa, Albert C.S. Tana, C. Quanc, „*Non-destructive characterization of resin-based filling materials using Electronic Speckle Pattern Interferometry Dental Materials”* (2004) 20, 377–382 http://intl.elsevierhealth.com/journals/dema
38. John P. Barranger, *„Two-Dimensional Surface Strain Measurement Based on a Variation of Yamaguchi's Laser-Speckle Strain Gauge”* - NASA Technical Memorandum 103162

ZASTOSOWANIE PROSZKÓW LUMINESCENCYJNYCH W CYFROWEJ FOTOGRAFII PLAMKOWEJ

Do generacji obrazów plamkowych wykorzystano proszek luminescencyjny naniesiony w niewielkiej ilości na powierzchnię próbki i pobudzany do świecenia promieniowaniem UV. Uzyskano drobnoziarniste struktury plamkowe (speckle pattern) o bardzo wysokim kontraście i małym rozmiarze plamek, których kształt w przeciwieństwie do speckli laserowych jest kołowy, co ma istotne znaczenie dla skuteczności zastosowanych metod cyfrowej analizy obrazu. Pomiaru przemieszczeń i odkształceń dokonano poprzez cyfrową rejestrację obrazu i jego analizę przy użyciu procedur korelacyjnych. Wyniki zostały przedstawione poglądowo w postaci bitmap oraz w sposób bezpośredni w postaci tablic i wykresów. Opracowana metoda badawcza została przetestowana na płaskich próbkach drewnianych poddanych zginaniu trójpunktowemu.

Słowa kluczowe: metrologia plamkowa, speckle elektroniczne, fotografia plamkowa w świetle białym, eksperymentalna analiza odkształceń, analiza obrazów plamkowych, Technika proszkowa, proszki luminescencyjne

DOI: 10.7862/rf.2019.pfe.2

Received:08.03.2019
Accepted:08.05.2019

A.A. MIKHAL[1]
D.V. MELESHCHUK[1]
Z.L. WARSZA[2]

APPLICATION OF THE HYBRID BALANCED RATIOMETRIC MEASUREMENT METHOD IN THE HIGH-PRECISION AC THERMOMETRY BRIDGES

The paper article describes the circuit of an automatic AC bridge for high precision temperature measurements using a standard platinum SPRT sensor. An original method for measuring the impedance parameters of SPRT sensor which allows to carry out the measurement process without loss of accuracy, is described in detail. This measurement method is proposed to name as hybrid method. It is a combination of a balanced method for rough compensation of the circuit and a ratiometric method which accurately measures the ratio of two values of the imbalance signal, before and after its known change. With this method, the measuring circuit also does not require a circuit to compensate for the reactive component of the SPRT sensor impedance. The inductive voltage divider with lower number of digits is needed only for the coarse compensation. This circuit is simpler and at lower cost of the hardware resources allows to achieve the same accuracy as the most accurate thermometric bridges with fully balanced circuits

Keywords: high precision temperature measurement, AC bridge, balanced-ratiometric measurement method, hybrid method

INTRODUCTION

Modern trends in improving the metrological support for temperature measurements are associated with a new definition of the unit of measure of the Kelvin degree. The advantage of redefining this unit will be the advancement of the technique of direct measurements of the thermodynamic temperature in parallel with the methods described in the IST. However, it takes some time to introduce modern trends into practice. Therefore, the following conclusions are made in the CCC document: "Report to the CIPM on the importance of changing the definition of the base unit kelvin" [1]. «IST-90 in the foreseeable future will be used as the most accurate and reliable approximation of the thermodynamic scale ... In the

[1] Institute of Electrodynamics, National Academy of Science of Ukraine, Kiev, a_mikhal@ukr.net
[2] Industrial Research Institute of Automation and Measurement (PIAP) Warszawa, Poland, zlw@op.pl

foreseeable future, the key range of the scale -200 ... + 960°C will continue to be carried out with the help of platinum resistance thermometers.»

At present, according to IST-90, temperatures in the range between the triple point of equilibrium hydrogen (13.8033 K) and the solidification point of silver (961.78°C) are carried out using standard platinum thermal resistance transducers (SPRT). Measurement of the value of the informative parameter (active resistance SPRT) is performed on a constant or alternating current. In most cases, the SPRT is connected as one of arms of an AC bridge. Since the error of interpolation of IST-90 is 0.00013 K, the thermometric bridges should have an error, brought to the end of the range, not worse than (1-3) 10^{-7}. Such a measurement error is realized using AC bridges with voltage (or current) dividers with close inductive coupling (IVD) as scaling converters.

Practical application of specialized thermometric circuits with inductive dividers begins with AC axes of Hill, Gibbings, Furd [2-4]. The main requirements for them were: high accuracy of the arm ratios and an effective four-clamp connection of the standard measure and the thermometer. Further progress in increasing the accuracy of measurements was the use of two-stage [5, 6] and multistage transformers. The best automatic thermometric AC bridges of ASL company (models F18, F900) or Tinsley (model 5840C) are built using such schemes. Obviously, IVD is the main part of these devices and determines the complexity and cost of the bridge and other instruments needed in the lab stand.

This article describes the semi balanced method of measuring only the resistance component of the impedance of SPRT sensor. This method allows to simplify the structure of the inductive voltage divider in precision AC thermometric bridges.

Functional diagram of the thermometric AC bridge

The functional diagram of high precision bridges as for example type F18 or F900 ASL [12] is presented in Fig. 1. To obtain the sensitivity needed in high precision temperature measurements, the inductive divider (winding m_1) must contain 7-8 decades. Note that, on an alternating current, the impedance ($Z_x \equiv Z_T$) of SPRT sensor has a two-element serial inductive equivalent circuit

$$Z_T = R_T + j\omega\omega_T = R_T + jQ_T = R_T\left(1 + jtg\,\varphi_T\right) \tag{1}$$

where: $tg\,\varphi_T$ is the tangent of the phase angle, i.e. the ratio of the reactive component Im (Z_T) to active component Re(Z_T), ω_T is the frequency of the bridge circuit andQ_T is the reactance.

To eliminate the influence of the reactive component on the sensitivity of the instrument, additional compensation circuits are necessary. In models F18 and F900, this problem is solved by connecting an additional current source $I_{\mathrm{Var}.Q}$ to point A - Quadrature Servo Range. Its phase must differ from the phase of generator G strictly by 90°. The error must not exceed the LSB (least significant bit)

of the inductive divider. Therefore, the current source $I_{Var,\,Q}$ is a complex module. For a further description of the method, another circuit for compensating the quadrature impedance parameter of SPRT sensor it is convenient to use. It is usually applied in universal RLC bridges. The circuit contains a multi-decade voltage divider with an adjustable number of turns m_2 and a quadrature phase shifter (QS), which provides a phase shift of the winding voltage m_2 by an angle of $\pi/2$ (conversion factor - j). The compensation circuit is connected between points B and C - in series to the voltage comparison circuit. Instead of an equilibrium detector, a vector voltmeter VV is used. Thus, the detector of the balance in precision thermometric bridges is a vector device. This device makes the thermometric bridge more complex and expensive. The AC-bridge complexity depends on two components. Firstly, it is the main inductive divider with secondary winding m_1 of 6-8 decimal decades. Secondly, it is an additional divider (winding m_2) and a precision phase shifter (QS).

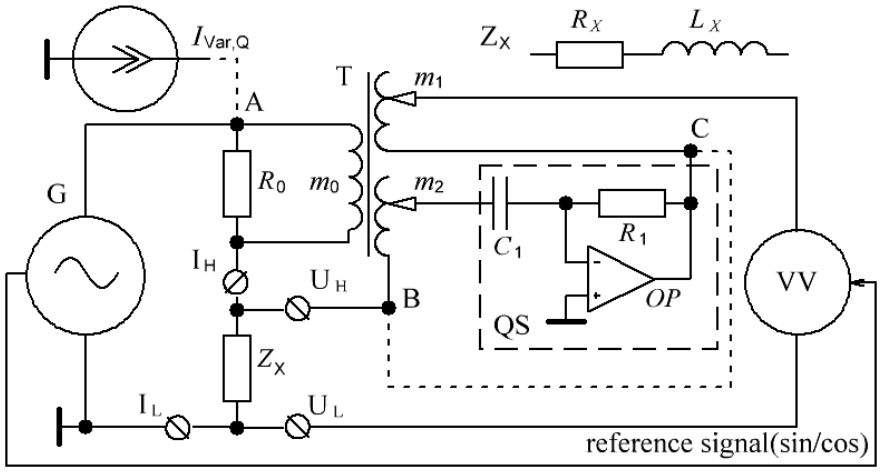

Fig. 1. Functional diagram of the measuring circuit of AC bridge (R_0 is the standard resistor)

Hybrid measuring method

The combined balanced-ratiometric method, called below shortly as hybrid method, eliminates the additional divider (winding m_2) and substantially simplifies the main divider (winding m_1). To achieve such results, a priori information on the phase characteristics of the SPRT is an important condition, i.e. the value of the $\mathrm{tg}\varphi_T$ parameter at the maximum operating frequency of different SPRT types. Frequency characteristics of SPRT, which are often used in Ukraine, will be presented below.

The hybrid method is based on two other well known methods. This is the method of balancing and the method of ratiometric transformation of two signals before and after their variation. Therefore, the hybrid method contains two stages.

Firstly, the bridge is balanced by an inductive divider m_1 with a limited resolution. Evaluation of the unbalance signal at this stage determines simultaneously the control codes of the converter and the values of the highest digits of the measurement result. On the second stage the measurement result is refined. Evaluation of the unbalance signal at this stage only determines the values of the least significant bits of the measurement result. At both stages, the unbalance signal is estimated by means of a ratiometric transformation. Its essence consists in the formation of a variation test impact with the help of IVD and calculation of the bridge disequilibrium from the ratio of the unbalance signals before and after the variation. The use of the signal ratio makes it possible to exclude several errors introduced by the elements of the measuring device. This method is called "variational" by its authors [7]-[9]. It was first used to correct the error of transformer bridges in measurements of high-resistance capacitive objects with a parallel substitution circuit [8]. As an extrapolation method of balancing thermometric bridges, it is presented in [9].

Variational method of balancing the AC bridge

A vector voltmeter VV is used to measure imbalance output voltage U_D of the AC bridge and gives results of measuring two orthogonal components of it. If phases of the supply generator signal and VV voltmeter coincide, then these components are named: in-phase component U_S (sin) and quadrature component U_Q (cos).

$$U_D = U_S + j\,U_Q = IR_S\left(p + jq - \frac{Z_T}{R_S}\right) \tag{2}$$

where: $p = m_1/m_0$ and $q = m_2/m_0$ - initial adjustable parameters of the common-mode and the quadrature-mode signal component respectively; $I \equiv I_H$- operating current.

The transmission coefficient QS at a fixed frequency, for simplicity, is equal to unity, i.e. $\omega\tau = 1$ (τ is the time constant of Z_x).

In the initial (unbalanced) stage of the circuit, each adjustable parameter is the sum of two parts: with indexes: *B* corresponding to the balanced state and *E* for the unbalance state, i.e.:

$$p = p_B + p_E, \qquad q = q_B + q_E \tag{3}$$

When the circuit is in balance, $U_D = 0$. From (1) and (2) follows the balance condition

$$p_B + jq_B = R_T/R_S + jQ_T/R_S \tag{4}$$

The circuit imbalance is determined by the error of balance E, which is a vector quantity Then:

$$\boldsymbol{E} = p_E - \boldsymbol{j}q_E\,, \quad p_E = p - \frac{R_T}{R_S}\,, \quad q_E = q - \frac{Q_T}{R_S} \tag{5a,b,c}$$

The balance parts (p_B, q_B) of the controlled parameters determine the components of the impedance of the measured object Z_T:

$$R_T = (p - p_E)R_S = p_B R_S\,, \qquad Q_T = (q - q_E)R_S = q_B R_S \tag{6a,b}$$

In the first cycle the AC bridge circuit is balanced by the variational method, but not completely and the components of the balance error E_1 are determined.

1. The non-balance components (in-phase U_{S1} and quadrature U_{Q1}) of the initial signal U_{D1} are measured

$$U_{D1} = U_{S1} + jU_{Q1} = I\,R_S E_1 \tag{7}$$

2. The variation of the adjustable parameter p is performed by changing the number of turns of winding m_1. The value of the variation is equal to $p_{V1} = m_{MSB}/m_0$. As a rule, this value is equal to the unit of discreteness of the older decade.

3. The components (in-phase U_{S2} and quadrature U_{Q2}) of the received U_{D2} imbalance signal are measured:

$$U_{D2} = U_{S2} + jU_{Q2} = IR_S(E_1 + p_{V1}) \tag{8}$$

From the joint solution of (6a,b) and (7) the expression of error E_1 is obtained. As a vector quantity, this error contains the real A_1 and the imaginary part B_1.

$$E_1 = p_{V1}\frac{U_{D1}}{U_{D2} - U_{D1}} = p_{V1}(A_1 + jB_1) \tag{9}$$

After substitution of the equation (2) to (9) with the allowance of indices, expressions for the coefficients A_1 and B_1 can be received, i.e.:

$$A_1 = \frac{U_{S1}(U_{S1} - U_{S2}) + U_{Q1}(U_{Q1} - U_{Q2})}{(U_{S1} - U_{S2})^2 + (U_{Q1} - U_{Q2})^2}; \quad B_1 = \frac{U_{S1}U_{Q2} - U_{Q1}U_{S2}}{(U_{S1} - U_{S2})^2 + (U_{Q1} - U_{Q2})^2} \tag{10a,b}$$

4. From (5) and (9), the components of errors of regulated parameters are calculated as

$$p_{E1} = A_1 p_{V1}\,, \quad q_{E1} = B_1 p_{V1} \tag{11a,b}$$

Equations (11a,b) make it possible to obtain a coefficient that determines the degree of the non-balance stage expressed in terms of the variation activity. It is important to note that variation in the form of a change of the number of turns of the inductive divider has a potential high accuracy, which can exceed 0.1 ppm. The accuracy of (11a,b) calculations depends also on the LSB of the vector voltmeter. It is possible that this voltmeter LSB will be smaller than the LSB of inductive divider. Then the process of determining the components of the imbalance state can be iterative.

5. The values of controlled parameters of the measuring circuit determined on the first stage of balancing process are:

$$p_B = p - p_{E1}, \qquad q_B = q - q_{E1} \tag{12a,b}$$

The advantage of this method (equations 2-12) is due to a priori information about the impedance of the SPRT sensor. It is known that the reactive component Q_T of the impedance Z_T (1) is several orders of magnitude smaller than the active component R_T. Then the format of the number q_B, will be represented with zeros in the upper digits. For example, q_B = 0.000358. Zero values do not make any sense to write to the divider registers m_2 (Fig. 1). To comply with this requirement, we restricted the minimum discretization of the divider by the natural number N_{IVD}. The conditions are as follows:

$$10^{-N_{IVD}} < tg\varphi \text{ - for the divider with decade structure,} \tag{13a}$$

$$2^{-N_{IVD}} < tg\varphi \text{ - for the divider with the binary structure.} \tag{13b}$$

With an error of LSB of the inductive divider, we have the following relations: $B_1 \approx 0$ and $q_{B1} \approx 0$. Under conditions (13a,b), the quadrature divider m_2 and the phase shifter Q_S in the circuit of Fig. 1 can be eliminated. The results of calculations of the basic parameter p_{B1} are recorded in the registers of the inductive divider and in registers of the upper bits of the computing device. As a result of the first stage, the bridge will be balanced to within 0.5 LSB of the inductive divider.

6. At the second cycle of the measurement process, the signal of the bridge imbalance $0{,}5 \cdot 10^{-N_{IVD}}$ is amplified. The variation is accomplished by changing the number of turns of the minor decade $p_{V2} = m_{\mathrm{LSB}}/\mathrm{m}_0$ and operations 1-5 are repeated.

7. The value of the error E_2 and the balanced values of the adjusted parameters p_{B2} and q_{B2} of equations (12a,b) are determined, similarly as p_{B1} and q_{B1} of E_1:

$$E_2 = p_B - \frac{R_T}{R_S} - j\frac{Q_T}{R_S} = p_{V2}(A_2 + jB_2)$$

$$p_{E2} = A_2 p_{V2}, \qquad q_{E2} = B_2 p_{V2} \tag{14}$$

The accuracy of calculation of the error components and balance values adjusted in the second stage (by analogy with the first stage) depends on the variation and the digit capacity of the vector voltmeter. By analogy with the first stage, this accuracy is also high. Then it is possible not to balance the measuring circuit for the least significant bits of the divider m_1. This accordingly simplifies the construction of the inductive divider and the circuit. In this case, the calculated balanced values of the parameters p_{B2} and q_{B2} are recorded only in the low-order registers of the computing device. Therefore, the number of digits in the calculator is summed.

8. In general, the measurement result of the informative parameter can be represented in the form:

$$R_T = R_S \cdot (p - p_{E1} - p_{E2}) = R_S \cdot (p - A_1 p_{V1} - A_2 p_{V2}) \tag{15a}$$

$$Q_T = R_S \cdot (q - q_{E2}) = R_S \cdot (q - B_2 p_{V2}) \tag{15b}$$

The reactive component Q_T of a SPRT sensor is not a informative parameter. But the Q_T/R_T ratio can be used to control if the quadrature parameter of the SPRT impedance is not in the limited range. Thus, when a combined hybrid measurement method is used, the resolution of the voltage divider may not be as high as needed for the measurement result. It is enough when voltage divider determines only numbers of the highest digits of the measurement result. They are added to the lower orders, which are determined in the second cycle. This will simplify the design, reduce the dimensions, weight and also the cost of the device.

The high accuracy and linearity of this method is due to several factors.

a) The presence of the high accuracy normalized levels of dividing by IVD and the ratiometric processing of imbalance signals before and after the variation. This ensures the invariance to the working current and phase changes in the filters of the generator, amplifier and other modules.

b) The variation of the signal is formed by changing the number of turns of a particular decade, which provides a connection with the LSB of inductive divider. The accuracy of the ratio of the non-balance level and variation is determined by the accuracy of the ratio of numbers of turns. It can be less than 0.1ppm.

c) A transformer voltage divider with a close inductive coupling has potentially higher linearity in comparison with the discreteness. For example, the linearity of 4-decade division may be better than 0.1 ppm (7 decades). This method have been experimentally tested and has two weaknesses also.

Firstly, the variational method of balancing requires two measurements: before and after the signal variation. As the result of this method the RMS of the Gaussian noise in the signal will increase by $\sqrt{2}$ times. This can be compensated by expanding the sample for averaging.

Secondly, with the incomplete balancing, the influence of the resistance of the connecting wires will not be completely eliminated.

To create cryogenic bridges for operation at very low cryogenic temperatures, this method still requires further development.

Implementation of the hybrid method in AC bridge

The e hybrid method was used in the precision thermometric AC bridge CA 300 (Fig. 2) [8-11].

Fig. 2. Automatic bridge AC type CA 300

Some features of the construction of chains of equipotential protection and metrological support of this bridge are considered in [10, 11]. From experimental studies, it is known that the SPRT sensors with a nominal resistance of 0.6 to 25 Ω (types of VTS, PTS-10, ТСПН-4В ТСПН-4В) at a frequency of 100 Hz have a phase angle tangent of not more than 0.0003. The optimal situation occurs when the inductive divisor is binary. It is easy to show from (13b) that the minimum number of digits (for a given maximum value of tgφ) should be N =12. To test the method, in the CA300 bridge a 12-bit inductive voltage divider and a vector voltmeter with a 12-bit ADC have been used. Its scheme is shown in Fig. 3 (In Fig. 3 the temperature sensor is marked by symbol "R_t").

In the first cycle, the imbalance voltage (as a 12-bit equilibrium code) is written to the inductive divider registers and in the high order digits of the calculator. In the second cycle, the imbalance voltage is written only in the registers of the calculator as low-order bits. The microcontroller combines the data of the registers into a 24-bit format, carries out the necessary calculations for the system calibration and put the result on the display. A balanced AC bridges with an inductive divider of seven decades corresponds to this hybrid circuit.

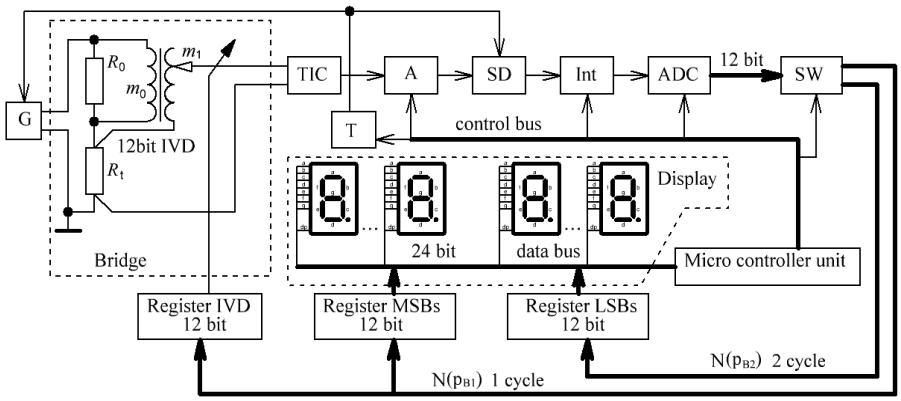

Fig. 3. A scheme working with combined - hybrid measurement method that provides a 24-bit effective number of binary digits: G - AC sinusoidal generator, TIC - matching transformer, A - amplifier, SD - two-channel (Re\Im) synchronous detector, Int - two-channel (Re\Im) integrator, ADC - analogue to digital converter, SW - switch, T - timing system.

An inductive voltage divider with a resolution of 12 bits (transformer m_1) for balancing the bridge is shown in Fig. 4.

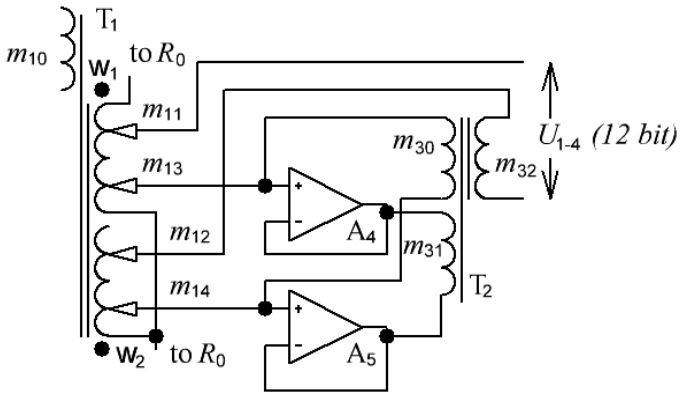

Fig. 4. Binary 12-bit inductive voltage divider IVD

The circuit contains two two-stage transformers T_1 and T_2. The weight coefficients of the windings w_1 and w_2 have a ratio of 1/8. Each of the windings m_{11} - m_{14} is switched by a system of electronic keys and realizes a voltage divider with a 3-bit capacity. Transformer T_2 has a transformation ratio of 1/64. Therefore, the summary voltage with a discreteness of 12 bits will be generated at the output of winding m_{14}. Transformers T_1 and T_2 are made on toroidal cores in the size 40 x 25 x 11 mm. The core material is amorphous cobalt (Co) iron with an initial magnetic permeability of μ=(1-2) 10^5. The divider has linearity no worse than 0.2 ppm at a working frequency of 125 Hz.

This new method based on the 12-bit ADC made it possible to realize the following main technical data of the bridge: LSD related to the full range - 0.06 ppm, linearity - 0.2 ppm, RMS at 0.05 Hz - 0.08 ppm. Such characteristics are comparable to those of the F18 ASL model [12]. Note that the bridge CA300 has dimensions of no more than 290 x 120 x 320 mm and a weight of not more than 6 kg. The level of the RMS indicates a certain reserve in the signal/interference ratio and is the possibility to add another decade. If a 16-bit ADC will be used, then with the same weight and dimensions is possible to get the parameters of an 8-decade bridge, for example equal to CTR9000 WIKA [12].

CONCLUSIONS

The tangent of the phase angle of standard platinum temperature sensors (SPRT) is very small [11,12]. Then the balancing process of measuring circuit of thermometric bridges it is possible to limit only for the active component of the SPRT impedance as the informative parameter about temperature. The circuit of AC bridge is simplified because it is transformed from a vector converter to a scalar converter.

The combined balanced-ratiometric method of the impedance measurement, named the hybrid method is proposed. This method is based on a variational method for estimating the bridge imbalance state, which allows you to significantly simplify the procedure of the AC bridge balancing.

The hybrid method allows also to use in AC measurement bridges a ratio transformer or an inductive divider IVD with a bit capacity smaller than is needed for the measurement result. The high resolution of the measurements will be retained by estimating the residual bridge imbalance. The high accuracy of measurements (LSD related to the full range - 0.06 ppm, linearity - 0.2 ppm, RMS at 0.05 Hz - 0.08 ppm.) by this method is provided by using the variational method of bridge balancing. It is based on the ratiometric transformation of signals before and after the variation and ensures invariance to phase changes of signals in the generator, amplifier and other bridge modules.

The use of a hybrid impedance measurement method significantly reduces hardware costs of the precision thermometric AC bridges manufacturing. At the same time, linearity and sensitivity remain the same as for fully balanced bridges with 7 to 8 decades of IVD.

LITERATURE

[1] Report to the CIPM on the implications of changing the definition of the base unit kelvin. Prepared by the task group TG-SI of the CCT. J. Fisher (chairman), S. Gerasimov, K.D. Hill, at al. 02 May (2007) http://www.temperatures.ru/pdf/Kelvin_ CIPM.pdf.

[2] Hill J.J., Miller A.P., *An A.C.* Double bridge with inductively coupled ratio arms for platinum resistance thermometry. Proc. IEE, **110** (2), 453 (1963)

[3] Gibbings D.L., *An alternating current analogue of the Kelvin double bridge*, Proc. IEE, **109C**, 307 (1962)

[4] Foord T.R., Langlands R.C., Binnie A.J., *Transformer-ratio bridge network with precise lead compensation*, Proc. IEE, **110** (9), p. 1693 – 1700 (1963)

[5] Cutkosky R., *An automatic resistance termometer bridge*. IEEE Transactions on Instr. and Measur. **IM – 29** (4), p. 330 – 333 (1980)

[6] Knight R.B., *Precision bridge for resistance thermometry using a single inductive current divider*. Euromeas-77; Europe conference on precise electrical measurements, London, p. 132-134 (1977)

[7] Grinevich F.B., Surdu M.N., *High-precision variational measuring systems of alternating current*, Kiev: Nauk. dumka, 192 p. (1989), (Rus.)

[8] Tretiak I.V., *Variational methods of correction of alternating current transformating bridge errors*. Abstract of a thesis Ph.D, NAS of Ukraine, Institute of Electrodynamics. Kiev, 18 p. (1991) (Rus.)

[9] Grinevich F.B., Surdu M.N., Mikhal A.A., Shvets T.V., Kromplias B.A., Meleshchuk D.V., *Precision bridge of alternating current for operation in 125-925 Hz frequency range*. Tekhnichna Elektrodynamika. Thematic issue "Problems of modern electrotechnics", **3**, 76–78 (2000) (Rus.)

[10] Mikhal A.A., Warsza Z.L., Electromagnetic Protection in High Precision Tri-axial Thermometric AC Bridge., R. Szewczyk et al. (eds.), Progress in Automation, Robotics and Measuring Techniques, vol. 3, Measuring Techniques and Systems, Advances in Intelligent Systems and Computing **352**, 147 -156 (2015) Springer International DOI: 10.1007/978-3-319-15835-8_17

[11] Mikhal A.A., Warsza Z.L., Simple Methods to Measure the Additive Error and Integral Nonlinearity of Precision Thermometric Bridges., R. Szewczyk et al. (eds.), Progress in Automation, Robotics and Measuring Techniques, vol. 3, Measuring Techniques and Systems, Advances in Intelligent Systems and Computing **352**, 157 -170 (2015) Springer International DOI: 10.1007/978-3-319-15835-8_18

[12] https://www.wika.co.uk/products_resistance_thermometry_bridges_en_co.WIKA

ZASTOSOWANIE HYBRYDOWEJ KOMPENSACYJNO-ILORAZOWEJ METODY POMIARU W WYSOKO PRECYZYJNYCH TEMPERATUROWYCH MOSTKACH AC

W artykule opisano oryginalną zasadę budowy układu pomiarowego automatycznego mostka AC (prądu przemiennego) do bardzo dokładnych pomiarów temperatury za pomocą wzorcowego platynowego czujnika SPRT. Wykorzystuje się oryginalną kombinowaną, tj. kompensacyjno-ilorazową metodę pomiaru, którą nazwano tu krócej: metodą hybrydową. Obejmuje ona połączenie metody kompensacyjnej do zgrubnego zrównoważenia układu i metody ilorazowej (*ratiometric*), którą wyznacza się stosunek dwu wartości sygnału nierównowagi, przed i po znanej jego zmianie. Układ pomiarowy nie wymaga stosowania obwodu do kompensacji wpływu reaktancji czujnika SPRT. Zmniejsza się też niezbędna liczba dekad dzielnika indukcyjnego kompensującego zgrubnie sygnał składowej rezystancyjnej czujnika. Układ taki pozwala w prostszy sposób i przy niższych

kosztach wykonania uzyskać tę samą dokładność co najdokładniejsze termometryczne mostki AC o układach całkowicie zrównoważonych.

Słowa kluczowe: dokładny pomiar temperatury, mostek AC, metoda hybrydowa, metoda kompensacyjno-ilorazowa

DOI: 10.7862/rf.2019.pfe.3

Received:17.04.2019
Accepted:05.07.2019

Tomasz SZCZEPAŃSKI[1]
Sylwia KUDŁA[2]

RESONANT TUNNELLING DIODE WITH MAGNETISED ELECTRODES

We analyse some basic properties of charge and spin transport in a semiconductor structure with an insulating barrier. In this system two semiconducting layers are separated by the insulator, creating a structure which is called a tunnel junction. The particles may pass through this junction according to the quantum tunnelling effect. By using two tunnel junctions with energy barriers made of insulating material, one can construct a quantum potential well . Inside the well the energy levels are quantised, which means that only discrete or quasi-discrete values of energy are allowed. Moreover, the probability of charge tunnelling through the system, which contains the potential well, depends on whether the energy of the incoming particles is in coincidence with the so-called resonant energy level. Such systems form the base of structures called resonant tunnelling diodes.

Keywords: resonant tunnelling diode, magnetic tunnelling diode, spintronics

1. INTRODUCTION: BASIC PROPERTIES OF A RESONANT TUNNELLING DIODE

Resonant tunnelling diodes (RTD) are one of the basic components of spintronics devices. They use the electrical and spin properties of electrons and they are important for current theoretical and experimental research. The fundamental phenomenon in a RTD is the tunnelling of particles which is a purely quantum effect. The particles can penetrate through the potential barriers by using their wave properties, allowed by the uncertainty principle. Therefore they can propagate through the classically forbidden region in which the energy of the electron is lower than the potential energy of the barrier. The solutions to Schrödinger's equation indicate that under the influence of an external magnetic field and voltage bias the intensities of tunnelling and contact currents depend on the resonance level energy and the geometrical characteristics of the structure [1].

The distinctive property of a RTD is that they are very sensitive to a small variation in the external bias voltage applied to the system. The structure consists

[1] Corresponding author: Tomasz Szczepański, Rzeszów University of Technology, Powstańców Warszawy 6, 35-959 Rzeszów, Poland, phone: (17) 865 1276, e-mail: tszczep@prz.edu.pl
[2] Sylwia Kudła, Rzeszów University of Technology, e-mail: s.kudla@prz.edu.pl

of several layers of materials. In the RTD system, the potential barriers could be thin layers of an insulator or semiconductor.

Usually one considers double potential barriers with one layer between the barriers, which is then the central part of the structure. This potential well is the region where the energy of the particles can have only discreet or quasi-discreet values. This means that the energy spectrum inside the well is quantised, this is the quantum well (QW). If the energy of an incoming electron is in coincidence with the energy of the quantum states inside the well, then the probability of the electron for tunnelling through the QW grows enormously.

This effect implies that the tunnelling properties of the structure depend on the energy values of the (resonant) levels inside the QW. The energies will also depend on any external magnetic field which could be applied to the system [2-4]. To do so, one can use a ferromagnetic material as an external layer outside one of the two barriers of potential. This material is usually a diluted magnetic semiconductor (DMS). The magnetic field acts on the spins of the electrons and makes the current that flows through the structure spin polarised. The magnetic field causes the splitting of the energy level into two spin channels, each of which is associated with one of two possible orientation of spin. This is because the eigenstates of the electrons have two possible spin orientations in the presence of the magnetic field. The spin splitting of the electron energy makes a difference to the tunnelling probability because only one of the two split levels can be in coincidence with the resonant level. This means that the RTD can be spin selecting materials for the transmitted electrons. Hence we can make the statement that RTD diodes are useful structures as spin filters.

One of the fundamental properties that are studied in magnetic junctions is the electric and spin current behaviour as a function of different parameters, for example the energy of the resonant level, the geometry of the structure, the influence of different materials (semiconductors, metals, superconductors), the magnetic moments of the system, the symmetry of the structure, and the spin polarisation of the current. One of the important phenomena that comes due to the spin current tunnelling is the induced magnetisation of the QW. Spin splitting of the resonant level causes nonzero magnetic moments in the QW level along with the spin accumulation properties of the RTD. This means the material can be magnetised due to the tunnelling of particles with spin from an external magnetised region. The dependence between magnetic field ratio and the scale of the spin splitting of the levels inside the QW are intensively studied properties of multilayered quantum systems. Experimentally, in all described cases, the conductance of the structure has strong resonance peaks as a function of the voltage, and the peaks can be controlled by external parameters like, for example, the magnetic field.

In a recent paper [5] the authors have shown that spin-selection in RTD can be controlled by changing the voltage. The study of a structure based on (Zn,Mn,Be)Se, with the DMS inside the well, showed that if one subjects the diode to an external magnetic field, the resulting spin splitting of the levels leads to

the splitting of the transmission resonance into two separate peaks. This could be used to design a voltage-controlled spin filter.

2. MANIPULATION OF THE MAGNETIC MOMENT IN A SINGLE TUNNEL JUNCTION

In the case of a single tunnel junction, there is an arrangement, in which two layers of a material (either semiconductor or metal) are separated by a thin layer of insulator [8,9]. At the interface of two layers we have a jump in the potential resulting from a difference in the band structures of the two materials. Often in electronic systems, we have to deal with two semiconductor interconnects (e.g. a semiconductor diode) or metal-semiconductor connectors (a so-called Schottky diode) in which two layers come in contact along a common plane and the energy barrier is formed by electric polarisation [10,11]. In our case, the electron transport through the coupling takes into account the effect of the magnetising of the structure and the resulting Zeeman splitting, and in particular the influence of the external magnetic field on the energy levels of the materials. An important role is played by the influence of the magnetic field on the tunnelling effect of the coupler. One must take into account the spin polarisation effect of the charge carriers and thus the influence of the magnetic field on the tunnelling [12]. In particular, attention is paid to the presence of the resonant energy levels, which significantly affect the probability of tunnelling charges.

If we take into account the spin polarisation of the resonant levels, we can consider the dependence of the efficiency of the spin transport on the intensity of the magnetic field covering the structure [13,6,7]. These tests are the basic element of accounts for two or more magnetic tunnelling systems. Thus, we have the ability to determine the characteristics of tunnel diodes, which are based on the flow of electric and spin currents through the tunnel barrier [14].

3. THE RESONANT TUNNELLING CONNECTOR

RTDs are the subject of intense study due to their specific characteristics and properties [14-16]. These devices have a high operating speed in excess of 2 THz (while in conventional CMOS systems speed is 215 GHz). The rapid development of RTD allows for a number of applications in high-resolution communications and high-resolution radar systems [17]. RTD, similarly to conventional diodes, have selective paths for the direction of charge transport. In the case of traditional complementary metal–oxide–semiconductor (CMOS) systems, the electrons flow through a special conducting channel in the system, however in the case of RTD the main effect, which makes transport of charge and spin possible, is tunnelling [18,19]. This transport is additionally strongly enhanced and depends on the quantised resonance energy level inside the cavity or well [1,7,20].

The tunnel diode includes a *p*-*n* junction, where both *p* and *n* regions are in a degenerate state [7]. There is a significant concentration of electrons in the conduction band of the *n*-type material with empty states in the valence band of the *p*-type material [10]. As a result, the Fermi level remains constant as long as the diode is in thermodynamic equilibrium without an external voltage applied. If the voltage is increased, the Fermi energy decreases in the *p*-type material and increases in the *n*-type. If the saturation area is very thin (< 10nm), then the electrons can easily flow through the barrier [21]. Depending on how many electrons are energetically compensated by the empty valence states of the *p* region, this current will either increase or decrease. As the potential difference increases, the current induced by the diffusion of charge carriers will increase the current flowing through the diode [22-24].

If a reverse external voltage is applied to the diode, the electrons in the *p* region are energetically compensated with the empty states in the *n* region, leading to a significant tunnel current in the direction of the applied voltage [21]. Current-voltage (or *I*-*V*) characteristics show negative differential resistance in the RTD. This means that in the range of voltages with these characteristics, an increase in the potential difference corresponds to a reduction in the current flowing through the diode. As a result, the current turns out to be a decreasing function of voltage. This property is particularly important in the context of applications because it allows one to correlate voltage-controlled logic states with the local maxima and minima of the current flow. In the case of a RTD, we have a QW with equal homogeneous contacts which can achieve a similar *I*-*V* characteristic. The diode consists of two highly-dispersive materials with a small energy barrier[8,9]. The structure of the diode reproduces a system composed of an emitter, a QW between two barriers, an energy gap and a collector area. Often, the materials used for this type of system consist of gallium arsenide compounds. The typical barrier width is about 5 nm and the barrier width ranges from 1.5 to 5 nm.

In the absence of an external voltage, most electrons and holes are deposited in the emitter and collector layers in a stationary manner. When an external voltage is applied to the system, an electric field is generated, which forces the electrons to move from the emitter to the collector through the dispersive states located in the potential well [2]. These energy states, through which electrons can tunnel, can mediate the conductivity. As more electrons in the emitter area have the same energy as quasi-bound states, more of them can overlap through the cavity, leading to an increase of current as a higher voltage is applied to the diodeo. As soon as the electric field reaches the intensity at which the energy level of the emitter electrons is in coincidence with the energy level of the resonant state, the current reaches its maximum value. The resonance tunnelling occurs within the range of specific resonant energy levels associated with the dopant energy levels and the quantum cavity width [21]. As the external voltage applied to the diode rises, more and more electrons have too much energy to be able to tunnel through the resonant states, resulting in a falling current. As the bias increases, the current rises again

due to electron thermo-emitting. Incorporation of these two phenomena leads to the appearance of a valley on the *I-V* characteristics of the RTD [23,1]. RTDs have a significant advantage over conventional tunnel diodes. When a high reverse voltage is applied to the tunnel diode, a very high reverse current is generated [23]. Unlike conventional tunnel diodes, RTDs have the same type of doping and concentration of charge in the collector and in the emitter. This results in a symmetrical *I-V* curve when both the voltage and current are applied to the diode in the opposite direction. As a result, the very strong "leakage" current that appears in a normal tunnel diode is eliminated in the RTD. This makes resonant tunnel diodes promising structures as a correction elements [13]. This system is characterised by low resistance and short travel times.

4. MODEL

We consider a structure consisting of several layers of semiconductors, with a tunnel junction as shown in Fig. 1. The dashed line in the QW of ZnSe corresponds to the energy level E_0. The layer in the left side of the structure, $x<0$, is based on a DMS.

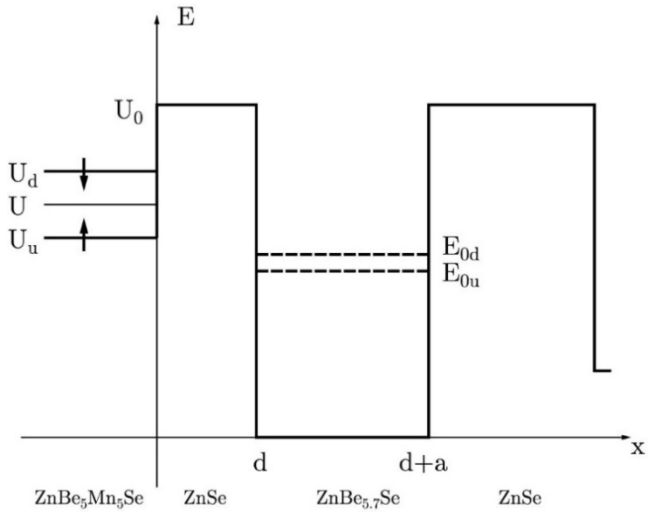

Fig. 1. Model of the multilayer structure with two potential barriers, where $U_{u,d}$ refers to electrons with spins up and down respectively, and U_0 is the potential barrier.

There is a spin splitting of the energy level in the layer due to a magnetic field. We can consider tunnelling of states into the rectangular QW restricted by two barriers both of the same potential height. First, we use Schrödinger's equation to get the wave function for the structure in the area $d < x < d+a$. Then we consider

the non-equilibrium problem, in which the plateaus of the top of the potential barriers are becoming oblique. In this structure, the potential energy is a function of the coordinate x. This case is useful for finding the magnetization inside the QW when there is a current through the structure. We used numerical calculations to find the current inducted magnetization as a function of the bias. The results demonstrate a strong influence of the magnetic field in small extent of the bias. We use experimental data for a five-layers structure.

We also used the results of numerical calculations to demonstrate the relation between the magnetic field and the energy level for four different values of the width d of the barrier. The width of the barriers was approximately $d = 1.5\times10^{-7}$ cm, the distance between them, which scales the well about $a = 2.5\times10^{-7}$ cm. The height of the barriers was $U_0 = 0.126\times10^{-12}$ J. The spin splitting inside the well is a consequence of the splitting in the DMS. We discuss the situation in which the energy level on the left side of the structure is lower than the height of the barrier at the interface at $x=d+a$, hence we are able to discuss it for realistic values of the parameters.

5. MAGNETIZATION IN A MAGNETIC FIELD

We assume that the diluted magnetic semiconductor (DMS) is located at $x < 0$. In the DMS, there are a large number of magnetic ions but the interaction between the magnetic moments of these ions is assumed to be very small, so that the moments are not ordered, and the average magnetization at $H = 0$ is zero. If the external field H acts on the DMS, it leads to the ordering of the moments, and the average magnetization M is nonzero. The relation between the magnetization M and magnetic field at finite temperature T is given by the equation [25]

$$M = xN_0 g\mu_B J B_S\left(\frac{g\mu_B JH}{kT}\right) \tag{1}$$

where $x = N_i/N_0$ is the relative density of magnetic ions (N_i is the concentration of magnetic ions and N_0 the number of sites in the crystal lattice), g is the Landé factor, μ_B is the Bohr magneton, J is the magnetic moment of a magnetic impurity, and $B_J(x)$ is the Brillouin function

$$B_J(x) = \frac{2J+1}{2J}coth\left(\frac{(2J+1)x}{2J}\right) - \frac{1}{2J}coth\left(\frac{x}{2J}\right) \tag{2}$$

The interaction between a free electron of spin 1/2 with the average magnetization M leads to the Zeeman splitting of the conduction band, which can be presented as

$$U_{u,d} = U(0) \mp \frac{1}{2}xN_0\alpha J B_J\left(\frac{g\mu_B JH}{kT}\right) \tag{3}$$

where α is a constant and $U(0)$ is the energy of the bottom of the conduction band at H=0. The value of $N_0\alpha$ is the exchange constant of the conduction electrons and $U_{u,d}$ refers to electrons with spin up and down,respectively. In this approach we neglect the interaction between magnetic ions.

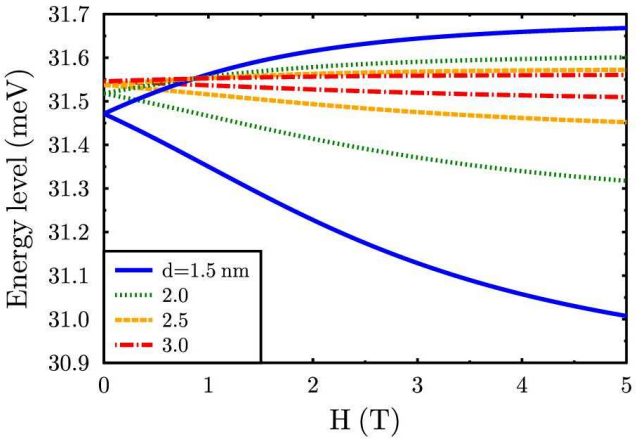

Fig. 2. Level positions as a function of magnetic field at T = 4.2K for different barrier widths d

We also have to take into account the density of states. In the one-dimensional case we can put the Fermi level in the place of energy E. At T = 0 the chemical potential is equal to the Fermi level, so if the energy E is lower than the Fermi level, the distribution function is equal one. In the three-dimensional case we calculate the magnetization and current integrals with respect to the wave vector **k**.

On the left side of the structure (Fig. 1) we choose the Fermi level to be higher than the value E of the energy for spin down oriented electrons. For that reason we consider tunnelling through both of the barriers. We solved numerically the dependence of magnetization M on energy for different values of temperature. The dependence of the energy levels on magnetic field H is presented in Fig. 2.

6. MAGNETIC SPLITTING OF THE QUANTUM LEVEL IN EQUILIBRIUM

We consider two different cases. If $U > E_0$, the penetration of the wave function of the states localised in the QW exponentially decays in the ZnBeMnSe layer. As a result, there is a quantisation level in the QW. Its energy can be calculated as a function of U (Fig. 3), where U is the conduction band edge in ZnBeMnSe. The variation of U is related to the magnetization in the DMS.

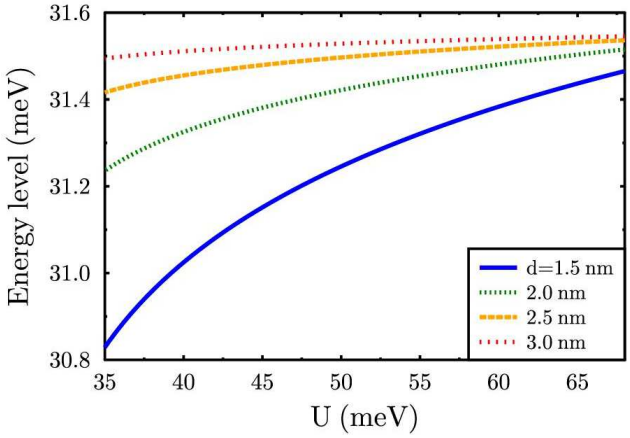

Fig. 3. The dependence of level position E_0 on U for different values of the barrier width d. The calculation is valid only for $E_0 < U$

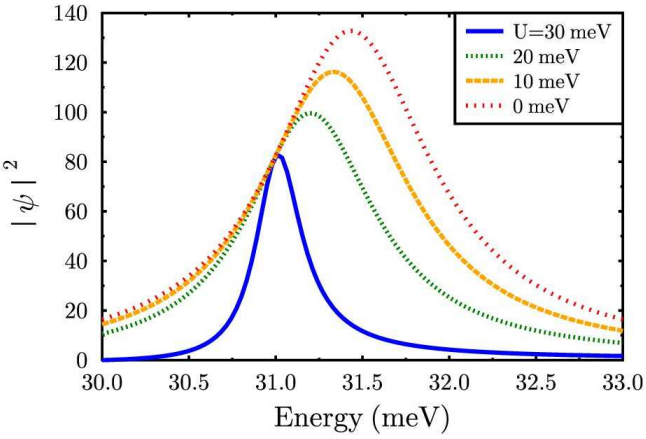

Fig. 4. The probability $|\psi|^2(E)$ for different U in the case of $U < E_0$

In the case of $U < E_0$ there is a tunnelling from the level into the conduction band of ZnBeMnSe. The level is quasi-discrete since there are states with all energies $E > U$. We calculated the distribution $|\psi|^2(E)$ where ψ is the wave function inside the QW (at $x = 0$) (Fig. 4). The peak of the dependence on energy corresponds to the position of the quasi-discrete levels in the QW. The maximum of each curve goes to a higher E as U goes down. However, the luminescence can start from the lowest possible energy, i.e., from the energy U even though the density of states in the QW for $E = U$ is rather low.

7. CONCLUSIONS

The effect which makes RTD materials especially important for spintronics is the possibility to select currents associated with two spin orientations, namely the spin currents. The difference in probabilities for two spin channels leads to a spin splitting of the quantum well energy levels and causes the induced magnetization inside the RTD. The spin splitting of the resonant level gets larger as the magnetic field on the outside region of the barrier is getting stronger. The spin filtering properties of RTDs make them important elements or the manipulation of spin currents. By changing the configuration of magnetic moments, one can affect the spin transport properties, especially the spin polarisation of the current. We can also predict and study the value of magnetization induced inside the quantum well by the spin splitting of the resonant level. That means that RTD spin currents can be controlled and manipulated by a magnetic field acting on the DMS material. This makes such elements very important for spintronic devices.

REFERENCES

1. Kilgour M., Segal D., *Tunneling diodes under environmental effects*. Journal of Physical Chemistry C, 2015, 119, 25291.
2. Figueiredo J.M.L., Ironside C.N., Stanley C.R., *Electric field switching in a resonant tunneling diode electroabsorption modulator*. IEEE Journal of Quantum Electronics, 2001, 37, pp. 1547-1552.
3. Figueiredo J.M.L., Boyd A.R., Stanley C.R., Ironside C.N., McMeekin S.G., Leite A.M.P., *Optical modulation at around 1550 nm in a InGa- AlAs optical waveguide containing a InGaAs/AlAs resonant tunnelling diode.* Applied Physics Letters, 1999, 75, pp. 3443-3445.
4. Figueiredo J.M.L., Stanley C.R., Boyd A.R., Ironside C.N., *Optical modulation in a resonant tunneling relaxation oscillator*. Applied Physics Letters, 1999, 74, pp. 1197--1199.
5. Slobodskyy A., Gould C., Slobodskyy T., Becker C.R., Schmidt G., Molenkamp L.W., *Voltage-controlled spin selection in a magnetic resonant tunneling diode.* Physical Review Letters, 2003, 90, 246601.
6. Du G.X., Wang S.G., Ma Q.L., Yan Wang, R.C., Ward C., Zhang X.G., Wang C., Kohn A., Han X.F., *Spin-dependent tunneling spectroscopy for interface characterization of epitaxial Fe/MgO/Fe magnetic tunnel junctions.* Physical Review B, 2010, 81, 064438.
7. Zutic I., Fabian J., Das Sarma S., *Spintronics: Fundamentals and applications.* Reviews of Modern Physics, 2004, 76, 323.
8. Nozaki T., Tezuka N., Inomata K., *Quantum oscillation of the tunneling conductance in fully epitaxial double barrier magnetic tunnel junctions.* Physical Review Letters, 2006, 96, 027208.
9. Wang Y., Lu Z.Y., Zhang X.G., Han X.F., *First-principles theory of quantum well resonance in double barrier magnetic tunnel junctions.* Physical Review Letters, 2006, 97, 087210.

10. Schmidt G., Ferrand D., Molenkamp L.W., Filip A.T., Wees B.J., *Fundamental obstacle for electrical spin injection from a ferromagnetic metal into a diffusive semiconductor*. Physical Review B, 2000, 62, R4790(R).
11. Fert A., Jaffrès H., *Conditions for efficient spin injection from a ferromagnetic metal into a semiconductor*. Physical Review B, 2001, 64, 184420.
12. López R., Sánchez D., *Nonequilibrium spintronic transport through an artificial Kondo impurity: conductance, magnetoresistance, and shot noise*. Physical Review Letters, 2003, 90, 116602.
13. Chshiev M., Stoeffler D., Vedyayev A., Ounadjela K., *Magnetic diode effect in double-barrier tunnel junctions.* Europhys. Letters 58, 257 (2002); Journal of Magnetism and Magnetic Materials, 2002, 240, 146.
14. Tiusan C., Greullet F., Hehn M., Montaigne F., Andrieu S., Schuhl A., *Spin tunnelling phenomena in single-crystal magnetic tunnel junction systems*. Journal of Physics: Condensed Matter, 2007, No. 16.
15. Faure-Vincent J., Tiusan C., Bellouard C., Popova E., Hehn M., Montaigne F., Schuhl A., *Interlayer magnetic coupling interactions of two ferromagnetic layers by spin polarized tunneling*. Physical Review Letters 89, 107206 (2002); Erratum: Physical Review Letters, 2002, 89, 189902.
16. Herranz D., Aliev F.G., Tiusan C., Hehn M., Dugaev V.K., Barnaś J., *Tunneling in double barrier junctions with "hot spots"*. Physical Review Letters, 2010, 105, 047207.
17. Ling J., *Resonant Tunneling Diodes: Theory of Operation and Applications.* New York 14627, 1999.
18. Fukuma Y., Wang L., Idzuchi H., Takahashi S., Maekawa S., Otani Y., *Giant enhancement of spin accumulation and long-distance spin precession in metallic lateral spin valves*. Nature Materials, 2011, 10, pp. 527–531.
19. Sokolovski D., Siewert J., Baskin L.M., *Symmetry-assisted resonance transmission of identical particles.* Physical Review A, 2016, 93, 012705.
20. Yamauchi Y., Sekiguchi K., Chida K., Arakawa T., Nakamura S., Kobayashi K., Ono T., Fujii T., Sakano R., *Evolution of the Kondo effect in a quantum dot probed by shot noise.* Physical Review Letters, 2011, 106, 176601.
21. Figueiredo J.M.L., Ironside C.N., Stanley C.R., *Ultra-low voltage resonant tunnelling diode electroabsorption modulator*. Journal of Modern Optics, 2002, 49, 5, pp. 939--945.
22. Hung N.V., Mazzamuto F., Bournel A., Dollfus P., *Resonant tunneling diode based on graphene/h-BN heterostructure*. Journal of Physics D: Applied Physics, 2012, 45, 325104.
23. Saffarzadeh A., Daqiq R., *Quantum size effects on spin-tunneling time in a magnetic resonant tunneling diode*. Journal of Applied Physics, 2009, 106, 084308.
24. Han W., Pi K., McCreary K.M., Li Y., Wong J.J. I., Swartz A.G., Kawakami R.K., *Tunneling spin injection into single layer graphene*. Physical Review Letters, 2010, 105, 167202.
25. Kittel C., *Introduction to Solid State Physics*, John Wiley, New York, 2005.

REZONANSOWA DIODA TUNELOWA Z ELEKTRODAMI MAGNETYCZNYMI

Przedstawiono podstawowe własności transportu ładunku i spinu poprzez wielowarstwowe struktury półprzewodnikowe, zawierające warstwy izolatorów. Układ półprzewodników przedzielonych warstwą izolatora stanowi rodzaj złącza tunelowego, poprzez które cząstki przedostają się wykorzystując zjawisko tunelowania kwantowego. Za pomocą dwóch złącz tunelowych zawierających bariery energetyczne w postaci materiału izolatora, konstruujemy kwantową studnię potencjału. W jej obszarze poziomy energetyczne ulegają skwantowaniu, przyjmując wyłącznie wartości dyskretne lub quasi-dyskretne. Ponadto prawdopodobieństwo tunelowania ładunków przez układ zawierający studnię potencjału zależy od tego czy energia padających cząstek znajduje się w koincydencji z dozwolonym w jamie tzw. rezonansowym poziomem energetycznym. Tego typu systemy stanowią podstawę funkcjonowania tzw. rezonansowych diod tunelowych. Przeanalizowano zależności od różnych parametrów układu, takich jak energia poziomu rezonansowego, szerokość barier potencjału, oraz wpływ pola magnetycznego na elektryczne oraz spinowe własności transportowanych cząstek. Badania te mają kluczowe znaczenie w projektowaniu urządzeń na potrzeby spintroniki. Wykorzystują one polaryzację spinową prądu, akumulację spinu w studniach potencjału, manipulowanie spinem w układach elektronicznych przy wykorzystaniu pola magnetycznego oraz indukowanie magnetyzacji w obszarze studni kwantowej zawierającej rozszczepione spinowo poziomy rezonansowe.

Słowa kluczowe: rezonansowa dioda tunelowa, magnetyczna dioda tunelowa, spintronika.

DOI: 10.7862/rf.2019.pfe.4

Received 19.06.2018
Accepted 4.02.2019

Igor TRALLE[1]
Paweł ZIĘBA[2]

ON THE NEW TYPES OF COMPOSITE METAMATERIALS

This paper is the review of our study published in J Appl Phys **115**, 233509 (2014) and J Mater Sci **53**, 2034 (2018). In it, we examined the possibility of fabricating the metamaterial, which is both gyrotropic and of the simultaneously negative permittivity and permeability. Our idea was to use the three-component mixture of ingredients, where one of them is responsible for the negative effective permeability μ_{eff} of hypothetical metamaterial, while all three are responsible for the negative value of effective permittivity ε_{eff}. At first we considered the following composite: the first component was the "swarm" of single-domain ferromagnetic nanoparticles, immersed in a mixture of other two, silver and mercury cadmium telluride. Then, as fabrication of the $Hg_{1-x}\,Cd_x\,Te$ is related to using mercury which is very poisoning, we tried to exclude this material substituting it by $Pb_{1-x}\,Sn_x\,Te$. Additionally, taking into account that silver is relatively expensive material, we have also used Cu and Al particles as the cheaper substitute of it. We have shown by computer simulations that by the proper fitting of the parameters, e.g., the radius of nanoparticles, their magnetic moments, the relative concentration of ingredients, etc., it is possible to obtain the double-negative metamaterial, that is with negative refraction index in a relatively broad range of temperatures and magnetic fields. The last seems to be very promising in terms of practical applications of metamaterials.

Keywords: negative refraction index, three-component gyromagnetic metamaterials, single-domain ferro-magnetic nanoparticles, superparamagntism, Bruggeman approximation

1. INTRODUCTION

In recent years, we have been witnessed of the explosion of interest in a field of research, which is termed as metamaterials. This area of research is characterized by an exponential growth of a number of publications and it is a hopeless task to refer to even the most important of them in a short Introduction. However, to mention just a few, there are two monographs [1, 2] and the references therein. According to Ref. [1], the term "metamaterials" can be used in a more general, as well as in a more specific sense. In the more general sense, these are materials possessing "properties unlike any naturally occurring substance" or simply "not

[1] Faculty of Mathematics & Naturals Sciences, University of Rzeszow, Poland.
[2] Energy Business Intelligence System, Rzeszow, Poland.

observed in nature." More specifically, these are the materials with a negative refractive index, whose existence and properties were discussed for the first time by Veselago [3]. Many of the researchers apply the term ''metamaterials'' to composites which contain inclusions of certain resonance properties and characteristic sizes of less than the wavelength, such as highly conducting needles, split rings, spirals. In 1967 V. Veselago [3] considered theoretically the medium, which has simultaneously negative real parts of permittivity and permeability, Re [ε] and Re [μ], respectively. Veselago himself called these materials 'left-handed'; left-handedness here refers to the fact that, when the refractive index is negative, the electric field vector E, the magnetic field vector H, and the wave-vector k of a plane wave make a left-handed triad. Since the term left-handedness sometimes is confused with chirality, it is not universally accepted among the researches. In the nice paper [4] Agranovich briefly discussed how people came to the understanding of the phenomenon and clearly pointed out that negative refraction occurs at the interfaces as a natural consequence of the negative group velocity of waves propagating in one of the media. It is worth mentioning that there is no unanimity as for the term negative group velocity materials also. Some authors prefer the term negative phase velocity materials. This is because in case of such materials the phase velocity and group velocity are directed against each other and which direction is positive and which is negative is the matter of convention. The results of Veselago on the other hand, confirmed that this type of medium has to have the negative refractive index, and thereby could exhibit a lot of extraordinary optical properties. The necessary requirement for the material to become negative refractive index material, as it was shown by Veselago and others is the negativity of both the real part of permittivity and real part of permeability, that is why we decided to use in this paper the term double-negative metamaterial (DNMM). Despite the theoretically envisaged possibility for this type of materials to exist, there was no experimental evidence of metamaterials occurring in nature. In the end of 1990s, Smith et al. [5] and Pendry with co-workers [6] published the seminal papers, in which they have shown that these types of materials can be produced in totally artificial way in laboratory.

It is interesting to note that already in his very first publication, Veselago anticipated that negative refraction index materials (or negative phase-velocity (NPV) materials) could be searched among gyrotropic materials. Optical activity, which is the ability of the medium to rotate the polarization plane of electromagnetic waves, has always been a phenomenon of great importance to many areas of research. Mackay and Lakhtakia, [7] Pendry [8], and Tretyakov [9] predicted that a strong optical activity may result in the negative refraction. Consequently, artificial gyrotropic media have started to attract a lot of attention as potential candidates for achieving negative refraction [10–12].

It is worth mentioning that most of the proposed ever since designs of metamaterials were characterized by ever increasing sophistication of fabrication methods. Contrary to these, in our previous work [13], we proposed a relatively

simple way to produce metamaterial using the mixture of three ingredients, where the one was responsible for the negativity of Re [μ(ω)] and the other two for the negativity of Re [ε(ω)].

This paper comprises an excerpts of our papers published previously [13, 14], in which we addressed the issue of the possibility to fabricate three-component artificial composite gyrotropic metamaterial and demonstrate by numerical simulations, what are the domains (relative to the concentrations of individual components as well as to other important parameters) of its existence.

2. THE MODEL

Let us assume that we have a mixture of three materials, each having granular or powder form, such that the grain sizes are much smaller than the electromagnetic wavelength propagating in the medium. We are trying to match the properties of ingredients in such a way that ε, the dielectric permittivity of the composite would be determined by the three components, while μ, magnetic permeability mainly by one of them responsible for the magnetic properties of the mixture. Let us start from the third ingredient mentioned above, which by the assumption should determine the effective permeability of the hypothetical material and suppose it to be metal magnetic nano-particles (or grains; we shall use these two words interchangeably). We treat these metallic grains as immersed or dispersed in a weakly conducting matrix. If the metallic particles are supposed to be single-domain, then we can take into account only the orientational alignment of their intrinsic magnetic moments and do not need to take into account their induced magnetic moments, as it can be easily proved (see Ref. [15], Chap. 82).

The size of the single-domain particle depends on the material and contributions from different anisotropy energy terms. If we assume nano-particle shape to be spherical, then typical values for the critical radius *a* are about 15 nm for Fe and 35 nm for Co, for g – Fe_2O_3 it is about 30 nm, while for $SmCo_5$, it is as large as 750 nm [16]. Now we can treat the suspension of metallic grains as a kind of "frozen paramagnetic macromolecules," where the metallic nano-particles play the role of "macromolecules." The magnetic moments of these single-domain nano-particles at room temperature are distributed at random and we can describe their behavior in the framework of Langevin theory of paramagnetism. Note that the "swarm" of magnetic nanoparticles immersed into another medium was already considered in scientific literature and even the term for describing this situation was already coined, namely, superparamagnetism [17]. The point is that such system behaves like a paramagnet, with one notable exception that the independent moments are not that of a single atom, but rather of a single-domain ferromagnetic particle, which may contain more than 10^5 atoms.

Thus, in the external magnetic field $\vec{H}_0$, an averaged magnetic moment of the unit volume of such medium is equal

$$\vec{M}_0 = \chi_0 \vec{H}_0 \tag{1}$$

where $\chi_0 = (N\mu^2_0)/3k_B T$; N, k_B are the concentration of magnetic nano-particles and Boltzmann constant, respectively, and T is a temperature. Suppose now that we put this hypothetical material in an external magnetic field $\vec{H} = \vec{H}_0 + \vec{h}(t)$, where the second term is the time dependent magnetic field of the electromagnetic wave, propagating in the medium.

Then, the magnetization of the medium can be represented as $\vec{M} = \vec{M}_0 + \vec{m}(t)$, where the second term arises due to time dependent component of the magnetic field and the equation
of motion is of the form

$$\frac{d\vec{M}}{dt} = \gamma \vec{M} \times \vec{H} \tag{2}$$

where γ is the gyromagnetic ratio. Supposing $h(t) << H_0$ and $m(t) << M_0$ one can make the linearization of Eq. (2) and after some algebra (see for details [1]) one arrives at

$$\vec{m} = \chi \vec{h}_t - \vec{G} \times \vec{h}_t \tag{3}$$

where

$$\chi = \chi_0 \frac{\omega_0^2}{2i\Gamma}\left(\frac{1}{\overline{\omega}_1 - \omega} - \frac{1}{\overline{\omega}_2 + \omega}\right),$$

$$G = \chi_0 \frac{\omega_0^2}{2i\Gamma}\left(\frac{1}{\overline{\omega}_1 - \omega} - \frac{1}{\overline{\omega}_2 + \omega}\right) H_0 \ .$$

Here $\vec{h}_t$ is the component of $\vec{h}(t)$ perpendicular to $\vec{H}_0$, vectors $\vec{H}_0$ and $\vec{G}$ in Cartesian coordinates are of the form $\vec{H}_0 = (0, 0, H_0)$, $\vec{G} = (0, 0, G)$, $\Gamma = \tau^{-1}$ (τ is relaxation time), $\overline{\omega}_1 = -i\Gamma + \sqrt{\omega_0^2 - 2\Gamma^2}$, $\overline{\omega}_2 = i\Gamma - \sqrt{\omega_0^2 - 2\Gamma^2}$, ω - is the frequency of the electromagnetic wave incident of the medium and $\omega_0 = \gamma H_0$. Using Eq. (3), one can write down the next formulae for m_x and m_y, components of $\vec{m}$:

$$m_x = \chi h_x + iGh_y \ , \ m_y = \chi h_y - iGh_x$$

Introducing the tensor

$$\chi_{\alpha\beta} = \begin{pmatrix} \chi & iG & 0 \\ -iG & \chi & 0 \\ 0 & 0 & 0 \end{pmatrix},$$

one can rewrite the above expression (3) as

$$m_\alpha = \chi_{\alpha\beta} h_\beta \ , \ \alpha, \beta = \{x, y\}$$

The conditions $\chi_{\alpha\beta} = \chi^*_{\alpha\beta}$ and $\chi_{\alpha\beta}(\vec{H}_0) = \chi_{\beta\alpha}(-\vec{H}_0)$ mean that the medium is gyrotropic [15]. Following the line of reasoning of Ref. [13], since our material is gyrotropic one, we can write down the formulae for the magnetic susceptibilities as follows:

$$\chi_\pm = \chi \pm G \ ,$$

$$\chi = \frac{\chi_0 \omega_0^2}{\omega_0^2 - 2i\omega\Gamma - \Gamma^2 - \omega^2}, \ G = \frac{\chi_0 \omega\omega_0}{\omega_0^2 - 2i\omega\Gamma - \Gamma^2 - \omega^2}$$

These two susceptibilities correspond to two possible circular polarizations of electromagnetic waves which are the eigenmodes of the gyrotropic medium.

In general, the propagation of light in gyrotropic medium is rather complicated and for the medium characterized by the magnetic susceptibility tensor mentioned above it will be considered elsewhere. But the situation becomes more lucid and simple when the wave vector of light is aligned along external magnetic field. Then it turns out, that in such medium two circularly polarized waves with $\vec{k} \parallel \vec{H}_0$ propagate which are characterized by two refraction indices. Thus, for this alignment we can consider the medium as isotropic except the two waves propagate in it.

Then, the expressions for real and imaginary parts of these magnetic susceptibilities, (χ_+ and χ_-) are of the form:

$$\mathrm{Re}\,[\chi_+] = \frac{\chi_0\omega_0\,(\omega_0^2 - \Gamma^2 - \omega^2)(\omega_0 + \omega)}{(\omega_0^2 - \Gamma^2 - \omega^2)^2 + 4\omega^2\Gamma^2},$$

$$\mathrm{Im}\,[\chi_+] = \frac{2\chi_0\omega_0\omega\Gamma(\omega_0 + \omega)}{(\omega_0^2 - \Gamma^2 - \omega^2)^2 + 4\omega^2\Gamma^2},$$

$$\mathrm{Re}\,[\chi_-] = \frac{\chi_0\omega_0\,(\omega_0^2 - \Gamma^2 - \omega^2)(\omega_0 - \omega)}{(\omega_0^2 - \Gamma^2 - \omega^2)^2 + 4\omega^2\Gamma^2},$$

$$\mathrm{Im}\,[\chi_-] = \frac{2\chi_0\omega_0\omega\Gamma(\omega_0 - \omega)}{(\omega_0^2 - \Gamma^2 - \omega^2)^2 + 4\omega^2\Gamma^2}.$$

The idea of the subsequent calculations (see for details Ref. [13, 14]) is the following. First, the 'swarm' of magnetic nanoparticles can be treated as paramagnetic in the frame of Langevin theory of paramagnetism, because in the absence of an external magnetic field their magnetic moments are distributed at random. Being placed in magnetic field, magnetic moments of individual grains, treated in terms of classical physics start to precess, that is why the frequency domain where Re [$\mu(\omega)$] < 0 appears in the vicinity of resonance ($\omega_0 \approx \omega$). Second, being in external magnetic field the whole ensemble behaves as gyrotropic material. Third, the magnetic moments of single-domain ferromagnetic nanoparticles are huge in comparison with atomic magnetic moments, that is why the 'swarm' of ferromagnetic nanoparticles forms 'super-paramagnetic'. As a result, the frequency ω_0 can be made greater in order to look for such frequency domains, where the dielectric permittivity and magnetic permeability are simultaneously negative.

As it was mentioned in the Introduction, in Ref. [13] for one of the mixture components was chosen $Hg_{1-x}Cd_xTe$ semiconductor compound. The reasoning behind this choice was the following. The electrical properties of this material are crucially dependent on cadmium concentration x. If $x = 0$, that is in case of HgTe, the material is semimetal with energy gap $E_g < 0$, while in case of $x = 1$ (CdTe) material becomes semiconductor with wide energy gap of about 1.5 eV at 300 K. Thus, changing the concentration of cadmium, one can change the energy gap, and hence the concentration of electrons. In terms of our model, it means that one can pass smoothly and continuously from Lorentz model for dielectric permittivity, where the electrons are almost tightly bounded to Drude model, where they are almost free to move. As a result, cadmium concentration becomes an important parameter of the model; by means of it–among others–one can control the frequency range where the real part of dielectric permittivity can be made negative and forced it to be overlapped with the frequency domain, where magnetic permeability is negative.

3. CALCULATION OF EFFECTIVE PERMITTIVITY AND PERMEABILITY

In our calculations of the effective permittivity and subsequent computer simulation of the hypothetical metamaterial, we consider a mixture consisting of three components: silver, mercury cadmium telluride $Hg_{1-x}Cd_xTe$ (here, x denotes a cadmium fraction), and the third one, which is the aforementioned "swarm" of magnetic nano-particles. We denote the permittivity of each component as $\varepsilon_1(\omega)$, $\varepsilon_2(\omega)$ and $\varepsilon_3(\omega)$, respectively, which depends on the angular frequency ω. It is known that there are several alternative approaches to the description of effective macroscopic characteristics such as the conductivity, permittivity, etc., of the composite media. Among them are Maxwell-Garnett theory also known as Clausius-Mosotti approximation [18-20] and the Bruggeman approximation often called as the effective medium theory [21] (see also Ref. [1]). We choose for our purposes the last one, because the Bruggeman theory is most widely known and used to calculate an effective permittivity of a composite medium. Its main asset is that all ingredients of a mixture by assumption are treated on the same footing in a symmetric way and none of them plays a privileged role. In this approximation, the effective permittivity can be calculated as the root of the following third-order algebraic equation (see Ref. [1] for details):

$$f_1\frac{\varepsilon_1-\varepsilon_{eff}}{\varepsilon_1+2\varepsilon_{eff}}+f_2\frac{\varepsilon_2-\varepsilon_{eff}}{\varepsilon_2+2\varepsilon_{eff}}+f_3\frac{\varepsilon_3-\varepsilon_{eff}}{\varepsilon 3+2\varepsilon_{eff}}=0.$$

As we consider a dissipative medium, we always choose the root of Eq. (13), which has a positive imaginary part. Using the permittivity values of particular ingredients (see [13]), we were able to calculate the effective permittivity of the mixture as well as its dependence on the frequency. As for the calculation of the permeability of mixture, we use the following formula:

$$\mu_{eff}=f_1\mu_1+f_2\mu_2+f_3(\chi+1)\approx f_{12}+(1-f_{12})(\chi+1),$$

where $f_{12}=f_1+f_2$. It can be easily shown that if the permeabilities μ_1, μ_2 of two other non-magnetic components are ≈ 1, which is the case, then this formula follows directly from the formulae obtained in the framework of the Bruggeman theory [22].

4. RESULTS OF COMPUTER SIMULATIONS

Our task now is to find the set of parameters: T – the temperature, $\vec{B}$ – external magnetic field, r – he radius of nano-particles, m – absolute value of the magnetic moment of nano-particles, x – the fraction of Cd in $Hg_{1-x}Cd_xTe$-com-

pound semiconductor, f_1, f_2, and f_3 fractions of the compounds in the mixture, and a range of frequencies for which the following inequalities are simultaneously fulfilled:

$$\mathrm{Re}\,[\mu_{eff}(\omega)] < 0,\ \ \mathrm{Re}\,[\varepsilon_{eff}(\omega)] < 0,\ \mathrm{Im}\,[\mu_{eff}(\omega)] > 0,\ \mathrm{Im}\ \ [\varepsilon_{eff}(\omega)] > 0.$$

As one can see, we have seven independent parameters to be controlled at the simulations and hence, a vast enough searching space, regardless the fact that all of them are bounded from above as well as from below. Our strategy can be briefly outlined as follows: first, we search for the range of frequencies where Re [μ(ω)] is negative and then we check if for the same frequency interval Re[ε(ω)] is negative The process of selecting the values of the model parameters are carried out in several sequential steps (for details, see [13]).

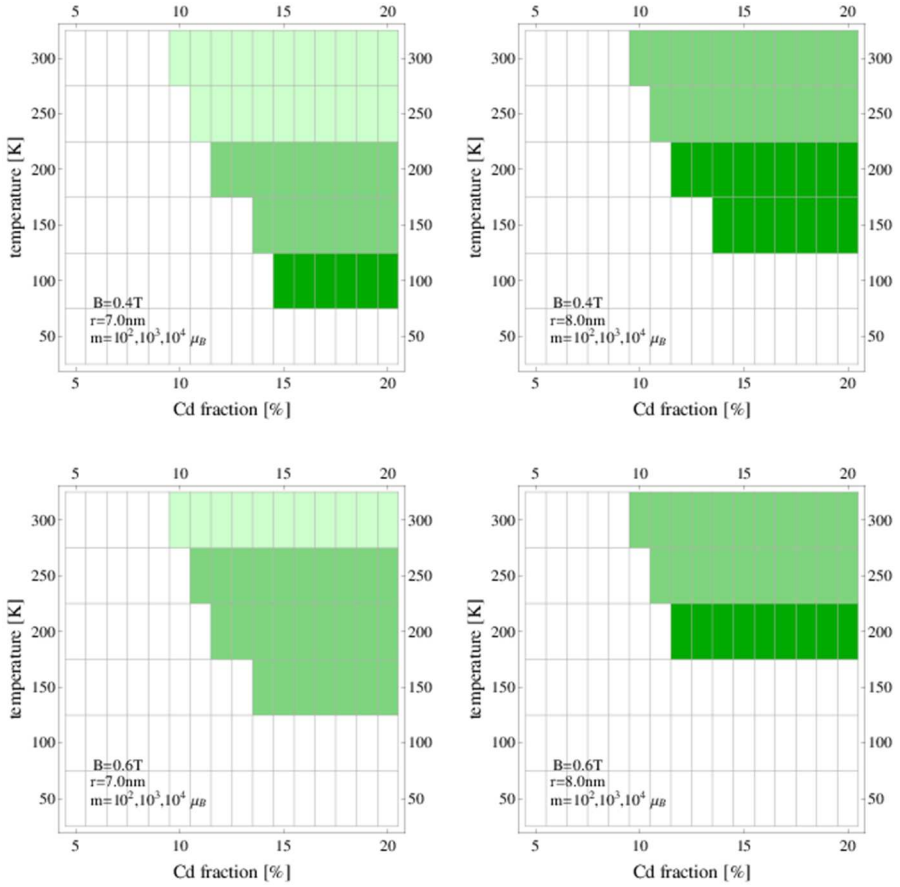

Fig. 1. The regions colored in different shade of green in *T*–*x* plane and for the different values of model parameters. *B*, *r*, and *m* (see in the main text) correspond to the domains in which at least one set of the filling factors f_1, f_2, and f_3 exists, such that the resulting mixture possesses Re [n] < 0

Figures 1–5 illustrate the results of our simulation. Figure 1 presents in *T–x* plane, for different parameter values of *B*, *r*, and *m*, the domains where at least one set of the filling factors f_1, f_2, and f_3 exists, such that the resulting mixture has the real part of the refractive index less than zero. The different colors have the following meaning: denote by D_1 the region colored in dark green, the domain colored in the intermediate shade of green as D_2, and the region colored in light green as D_3. Then, D_1 corresponds to $m = 10^2\ \mu_B$, $D_1 \cup D_2$ corresponds to $m = 10^3\ \mu_B$ and $D_1 \cup D_2 \cup D_3$ corresponds to $m = 10^4\ \mu_B$, where μ_B – Bohr magneton. We observe that for the greater values of nano-particle magnetic moment, the existence domain of metamaterial becomes larger.

The similar results are presented in Fig. 2 and Fig. 3, where different parameter values of *B*, *r*, and *m*, correspond to the domains where at least one set of the filling factors f_1, f_2, and f_3 exists, such that the resulting mixture has the real part of the refractive index less than zero. Now however, $Hg_{1-x}Cd_xTe$ is substituted in a mixture by $Pb_{1-x}Sn_xTe$ and silver is substituted by Al. The different colors have the following meaning: denote by D_1 the region colored in yellow, the domain colored in orange as D_2, and the region colored in red as D_3. Then, D_1 corresponds to $m = 10^2\ \mu_B$, $D_1 \cup D_2$ corresponds to $m = 10^3\ \mu_B$ and $D_1 \cup D_2 \cup D_3$ corresponds to $m = 10^4\ \mu_B$.

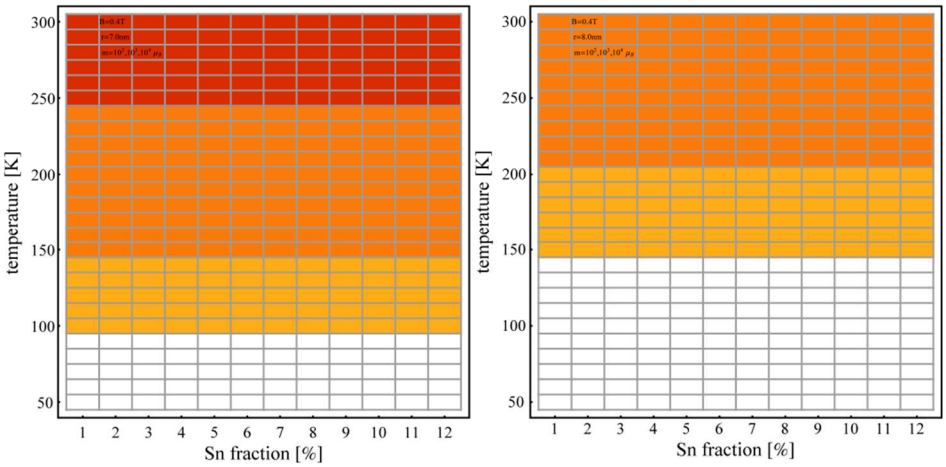

Fig. 2. The regions colored in red, orange and yellow (see text) in *T* - *x* plane and for the different values of model parameters for the mixture of $Pb_{1-x}Sn_xTe$, ferromagnetic nanoparticles and Al particles. *B*, *r* and *m* correspond to the domains in which at least one set of the filling factors f_1; f_2; f_3 exists, such that the resulting mixture possesses Re [n] < 0

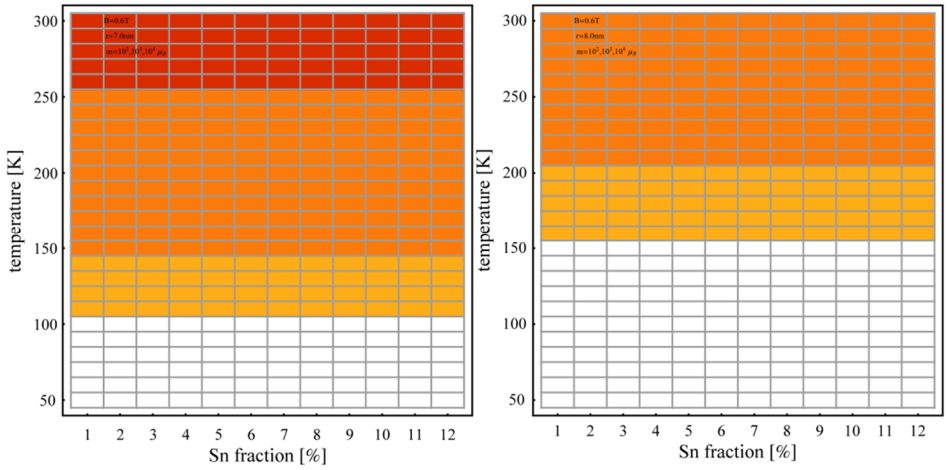

Fig. 3. The same as in Fig. 2, but for different values of *B*

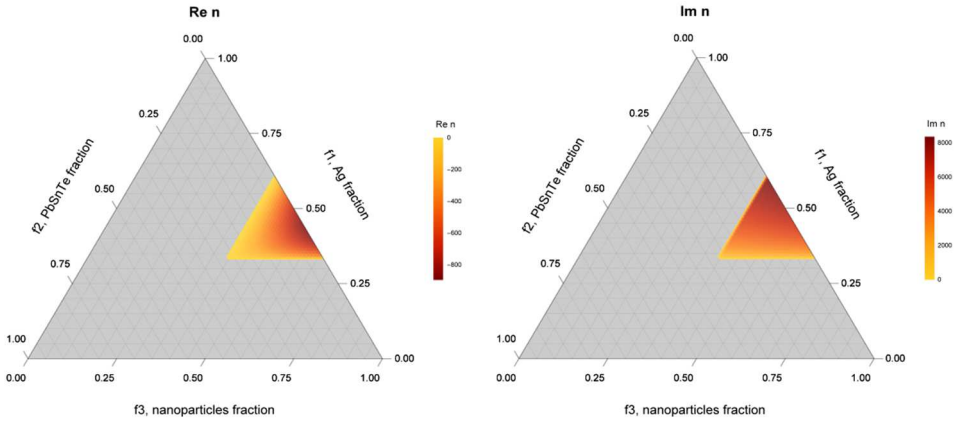

Fig. 4. Real and imaginary parts of the refractive index of the composite for selected cases presented on the ternary diagram. On each axis of the triangle, the relative contribution of individual components of the composite are indicated, which are expressed as the values of the filling factors f_1; f_2; f_3. The model parameters are : B = 0.2 T, r = 8 nm, m = 10^4 μ_B, T = 300 K, x = 0.08

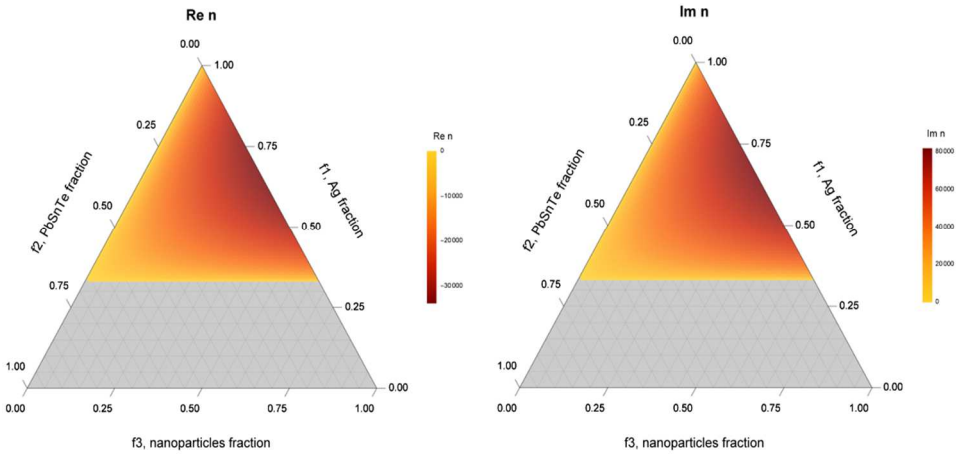

Fig. 5. The same as in Fig. 4, but for the model parameters B = 0.4 T, r = 8 nm, $m = 10^4$ μ_B, T = 300 K, x = 0.08

5. CONCLUSIONS

Up to now many metamaterial designs leading to a negative refraction index were proposed by the researchers. In 2000, it was shown experimentally that a metamaterial composed of periodically positioned scattering elements, all conductors, could be interpreted as showing simultaneously negative ε and μ in some frequency domain. An experimental observation of the negative refraction was reported for a metamaterial composed of wires and split-ring resonators deposited lithographically on the circuit board material [23]. All of the proposed ever since designs have their advantages as well as disadvantages, but it would be perhaps not an overstatement to say, that they are characterized by ever-increasing sophistication of fabrication methods. On the contrary, in our work [13], we proposed a comparatively simple way to produce a material which is at once gyrotropic and of negative-phase velocity. The idea is to make a mixture of three ingredients, where one of them would be responsible for the negativity of μ, while all three would be responsible for the negativity of ε. The first component of the mixture is the "swarm" of single-domain ferromagnetic nano-particles, immersed in a mixture of other two, silver and mercury cadmium telluride. The choice of silver is determined by the fact, that as it was shown, the permittivity of a mixture of silver and a dielectric material can be negative in some frequency domain. The other argument in favor of using silver is that it is a diamagnetic material. It means that considering the "swarm" of single domain ferromagnetic nano-particles suspended in a mixture containing silver, we can neglect the interaction between their magnetic moments and treat the whole mixture as superparamagnetic. The choice of mercury cadmium telluride is determined by the remarkable dependence of its energy gap on the fraction of cadmium in the compound. In its turn, it leads to the

strong dependence of the electron concentration on this fraction as well as on the temperature. It enables to adjust to each other two frequency domains where $\varepsilon < 0$ and $\mu < 0$ and make them simultaneously negative. In [13] , we carried out computer simulations in the frame of the proposed model in order to establish the domains of existence of such material, searching through a vast parameter space. We have seven parameters to be controlled in course of simulations, these are the temperature, external magnetic field, radius of nano-particles, their magnetic moments, fraction of cadmium in $Hg_{1-x}Cd_xTe$-compound, and the relative concentrations f_1, f_2, and f_3 of the components in a mixture. In total, there are eight parameters, but due to the relation $f_1 + f_2 + f_3 = 1$, only seven of them are independent. Despite as it seems, a relative simplicity of fabrication, if produced, such a metamaterial will show its disadvantages or limitations in use, too. First of all, a negative refraction can be achieved only if the material is in an external, although moderate magnetic field. In our calculations, B was restricted to ~ 0.8 T. On the other hand, in some circumstances it could be an advantage, since switching magnetic field on and off, one can trigger NPV-state on/off.

Another disadvantage is the use of $Hg_{1-x}Cd_xTe$, since its fabrication is related to using mercury, which is very poisoning. So, in the work [14] we substituted $Hg_{1-x}Cd_xTe$ by $Pb_{1-x}Sn_xTe$ and silver by Al and Cu, since they are also diamagnetic. On the other hand, silver is relatively expensive, while aluminum and copper are cheaper and have very similar conducting properties as silver. By computer simulations, we establish the domains where the material becomes negative refraction index material relatively to all parameters characterizing the mixture.

REFERENCES

1. W. Cai and V. Shalaev, *Optical Metamaterials: Fundamentals and Applications* (Springer-Verlag, Berlin, 2010)
2. L. Solymar and E. Shamonina, *Waves in Metamaterials* (Oxford University Press, New York, 2009)
3. V.G. Veselago, Sov. Phys. Usp. **10**, 509–514 (1968)
4. V.M. Agranovich and Y.N. Gartstein, Phys. Usp. **49**, 1029–1044 (2006)
5. Smith D.R., Padilla W.J., Vier D.C., Nemat-Nasser SS, Schultz S Phys Rev Lett **80**: 4284 (2000)
6. Pendry J.B., Holden A.J., Robbins D.J., Steward W.J., IEEE Trans Microw Theory Tech **47**:2075 (1999)
7. T.G. Mackay and A. Lakhtakia, Phys. Rev. E **69**, 026602 (2004)
8. J.B. Pendry, Science 306, 1353 (2004)
9. S. Tretyakov, J. Electromagn. Waves Appl. **17**, 695 (2003)
10. Y. Jin and S. He, Opt. Express **13**, 4974 (2005)
11. C. Monzon and D.W. Forester, Phys. Rev. Lett. **95**, 123904 (2005)
12. Q. Cheng and T.J. Cui, Phys. Rev. B **73**, 113104 (2006)
13. I. Tralle, P. Zięba, W. Paśko, J. Appl Phys **115**, 233509 (2014)

14. W. Paśko, I. Tralle, K. Majchrowski, P. Zięba, A. Çoruh, J. Mater Sci **53**, 2034–2044 (2018)
15. L. Landau and E. Lifshitz, *Electrodynamics of Continuous Media* (Addison-Wesley, MA, 1960).
16. D. Givord, Q. Lu, and M.F. Rossignol, in *Science and Technology of Nanostructured Materials*, edited by G.C. Hadjipanayis and G.A. Prinz (Plenum, New York, 1991), p. 635
17. J.L. Gittelman, B. Abeles, and S. Bozowski, Phys. Rev. B 9, 3891–3897 (1974)
18. O. Levy and D. Stroud, Phys. Rev. B 56, 8035–8046 (1997)
19. J.C.M. Garnett, Philos. Trans. R. Soc. London, Ser. B 203, 385 (1904)
20. R. Landauer, AIP Conf. Proc. 40, 2 (1978)
21. D.A.G. Bruggeman, Annalen der Physik 416(7), 636–664 (1935)
22. T. Mackay and A. Lakhtakia, Microwave Opt. Technol. Lett. 47, 313–315 (2005).
23. R.A. Shelby, D.R. Smith, and S. Schultz, Science 292(5514), 77–79 (2001).

NOWY TYP KOMPOZYTOWYCH METAMATERIAŁÓW

Praca stanowi przegląd prac autorów, opublikowanych wcześniej (*J Appl Phys* **115**, 233509 (2014) oraz *J Mater Sci* **53**, 2034 (2018)). W w/w pracach autorzy zbadali możliwość utworzenia metamateriału, który byłby jednocześnie giroskopowy oraz posiadał ujemne części rzeczywiste przenikalności magnetycznej i dielektrycznej. Ideą jest wykorzystanie w tym celu mieszanki trzech składników, z których pierwszy - to "rój" ferromagnetycznych nano- cząstek

Słowa kluczowe: ujemny współczynnik załamania, trójskładnikowy metamateriał giromagnetyczny, jednodomenowe ferromagnetyczne nano- cząstki, superparamagnetyzm, przybliżenie Bruggemana.

DOI: 10.7862/rf.2019.pfe.5

Received:29.01.2019
Accepted:06.03.2019

ADDITIONAL INFORMATION

The Journal annually publishes a list of reviewers: in the last issue of the quarterly - no. 4/2019 and on the website:
https://oficyna.prz.edu.pl/zeszyty-naukowe/physics-for-economy

The Journal uses as described on its website the procedure for reviewing:
https://oficyna.prz.edu.pl/zeszyty-naukowe/physics-for-economy/zasady-recenzowania/

Information for authors available at:
https://oficyna.prz.edu.pl/zeszyty-naukowe/physics-for-economy/informacje-dla-autorow/

Review's form available at:
https://oficyna.prz.edu.pl/zeszyty-naukowe/physics-for-economy/formularz-recenzji/

Instruction for Authors:
https://oficyna.prz.edu.pl/zeszyty-naukowe/instrukcja-dla-autorow/

Contact details to Editorial Office available at:
https://oficyna.prz.edu.pl/zeszyty-naukowe/physics-for-economy

Electronic version of the published articles available at:
https://oficyna.prz.edu.pl/zeszyty-naukowe/physics-for-economy

Circulation 25 + 40 copies. Publisher's sheet 3,81. Printer's sheet 3,50.
Manuscript completed in July 2019, Printed in July 2019.
Printing Publishing House, Powstancow Warszawy 12, 35-959 Rzeszow
Order no. 53/19

Physics for Economy

COOPERATING REVIEWERS – 2019

prof. dr hab. inż. Vitalii DUGAEV
prof. dr hab. inż. Mykhaylo DOROZHOVETS
dr hab. Paweł JAKUBCZYK, prof. URz
dr hab. inż Jerzy PISAREK, prof. AJD
prof. dr hab. Igor TRALLE

Physics for Economy

SCIENTIFIC BOARD

Physics for Economy

KOMITET REDAKCYJNY

Adres pocztowy i afiliacja Komitetu Redakcyjnego

Politechnika Rzeszowska
Wydział Matematyki i Fizyki Stosowanej
al. Powstańców Warszawy 6
35-959 Rzeszów, Polska

Informacje dla autorów
http://oficyna.prz.edu.pl/zeszyty-naukowe/physics-for-economy

Dane kontaktowe do wydawcy

Kierownik Oficyny Wydawniczej
mgr inż. Joanna BIENIASZ
Politechnika Rzeszowska
al. Powstańców Warszawy 12
35-959 Rzeszów
e-mail: jbie@prz.edu.pl
tel. +48 17 865 1195